AN ABSTRACT OF THE THESIS OF

Jose L. Pelegri for the degree of Master of Science in Oceanography presented on August 13, 1984.

Title: The Role of Inertial Oscillations in the Dynamics of Coastal Upwelling.

Abstract approved: Redacted for privacy
James G. Richman

A finite difference scheme is employed to solve the integral form of the momentum, continuity and heat equations, for a two layer ocean bounded by a coastline. The momentum equations include the turbulent dynamics and the time-dependent and nonlinear terms in both the cross-shelf and alongshelf directions. The system of equations is closed using a parameterization for the entrainment velocity proposed by Niiler and Kraus (1977), which has both the wind-stirring (Kraus and Turner, 1967) and the shear-mixing (Pollard, Rhines and Thompson, 1973) mechanisms.

DeSzoeke and Richman's (1984) semigeostrophic model, which eliminates inertial oscillations by forcing geostrophic cross-shelf dynamics, is modified to include the shear-enhanced mixing mechanism. By comparing the results from this model with those from our model, with and without the shear-mixing mechanism, we conclude that 1) inertial oscillations drive the horizontal volume flux divergence at the coast, 2) the shear-mixing mechanism plays a very important role during coatal upwelling, and 3) while the maximum contribution to this mechanism comes from the alongshore baroclinic jet, inertial oscillations also give a significant contribution far offshore from the front. It is concluded that any realistic model for coastal upwelling should include both inertial oscillations and the shear-enhanced mixing mechanism.

The Role of Inertial Oscillations in the Dynamics of Coastal Upwelling

by

Jose L. Pelegri

A THESIS

submitted to

Oregon State University

in partial fulfillment of
the requirements for the
degree of

Master of Science

Completed August 13, 1984

Commencement June 1985

APPROVED:

Redacted for privacy

Associate Professor of Oceanography in charge of major

Redacted for privacy

Dean of College of Oceanography

Redacted for privacy

Dean of Graduate School

Date thesis is presented August 13, 1984

Typed by researcher for Jose L. Pelegri

Con amor y gratitud:

a Monica, mis padres

y mi tierra.

AKNOWLEDGEMENTS

I am happy to thank Prof. James Richman for his guidance and enthusiasm throughout my stay in Corvallis, and particularly in the last months. Without his support this work would not have been possible. I am also very grateful to Eric Beals for his help in some of the computations.

I want to thank my fellow students and friends, whom have shared with me this period of my life, and have made of it an unvaluable experience.

My deepest thanks is for my wife, Monica Garcia, for her love, understanding, and encouragement at any moment.

My stay and studies at OSU have been fully supported by an scholarship from CEPET, Petroleos de Venezuela.

TABLE OF CONTENTS

LIST OF TABLES

LIST OF FIGURES

A.2 Cell structure showing the positioning of the 77 variables.

THE ROLE OF INERTIAL OSCILLATIONS IN THE DYNAMICS OF COASTAL UPWELLING

1. INTRODUCTION

The main elements in the dynamics of coastal upwelling are a surface offshore Ekman flow and a compensating onshore subsurface flow, linked by a region of horizontal divergence and vertical flow near the coast. These and other aspects of the problem have been carefully analyzed in the last decades (for reviews see Thompson, 1978, and Allen, 1980). Our purpose in this paper is to study in detail two elements which still have a high degree of uncertainty. First, we will be looking at the importance of inertial oscillations in the adjustment problem at the coast. Secondly, we will be concerned with the controversial issue of whether shear enhanced mixing is significant during upwelling, and what possible sources for this enhanced mechanism exist. Both topics are intimately connected.

Mixed layer models constitute a realistic approach to the study of coastal upwelling, and have the advantage of permiting the integral representation of the mixed layer dynamics (for a review on mixed layer integral models see Niiler and Kraus, 1977). Two main tools for

our analysis will be the recent integral models by deSzoeke and Richman (1984) and Richman and Allen (1984). DeSzoeke and Richman (1984), hereinafter DR, have employed the semigeostrophic approximation to formulate an appealing two-dimensional mixed layer model which produces strong horizontal gradients associated with an upwelling front propagating offshore. They show that the horizontal scale of this front is given by an internal Rossby radius of deformation based on their scaling for the problem. However, their formulation effectively eliminated all inertial oscillations, which causes the establishment of an offshore Ekman balance in an infinitesimal time. In DR's model entrainment is parameterized using the representation proposed by Kraus and Turner (1967), hereinafter KT, in which the wind acts as the source for turbulent energy in the upper layer.

In this paper we present a two-layer model which solves the full momentum equations in their integral form, allowing for turbulent exchange between layers. The problem is closed using the Niiler and Kraus (1977) representation for the turbulent kinetic energy equation, which includes both the KT mechanism and the shear mixing mechanism proposed by Pollard, Rhines and Thompson (1973) (hereinafter PRT). The inclusion of the time dependent terms in our model will permit us to study the role of the inertial oscillations in the dynamics of upwelling, both

in the modification of the divergence at the coast and in the enhancement of the shear mixing mechanism.

In the simple wind-forced inertial problem it can be shown that the divergence at the coast is reduced for times shorter than f^{-1} . Richman and Allen (1984), hereinafter RA, have used a non-entraining model to look at cases ranging from the inertial oscillation dominated problem to the semigeostrophic approximation and have obtained that the time that takes for the thermocline to upwell decreases until a value of approximately 0.7 λ_i/u_0 , where λ_i is the initial Rossby radius of deformation and u_0 is the Ekman velocity. The semigeostrophic approximation can be obtained as a limiting case of our model through the choice of a large value for $q_0=q^2(\Delta_i h_i)^{\frac{1}{2}}$, where λ_i and h_i are the non-dimensional initial values for the temperature difference between both layers and the upper layer depth, and q is a non-dimensional inertial frequency that arises from our scaling of the problem. Results for several values of q_0 are in agreement with the trend shown by RA, the effect of entrainment being to further advance the surfacing of the thermocline at the coast.

For all cases considered the shear production mechanism is important in the turbulent kinetic energy budget. The major local contribution comes from the strong alongshore jet which develops at the front.

Inertial oscillations have significant effect far offshore from the coastal region. A version of DR's model which includes this mechanism is implemented and gives confirmation to the above results.

Our model shows the formation and development of strong horizontal density gradients which propagate away from the coast. Offshore from this front the upper layer is warmer and deeper, and exhibits an open ocean regime consisting of an Ekman balance plus inertial oscillations. The frontal region is characterized by a strong alongshore jet, which resembles those analyzed by Csanady (1981). The region onshore from the front is essentially decoupled from the exterior. It corresponds to a zone of large entrainment with very little vertical structure. Maximum entrainment values occur at the coast , being driven by the large velocity divergence there. Large values also occur close to the front, where the upper layer shallows considerably and both wind stirring and shear velocity at the interface reach a maximum. The front itself moves offshore with the velocity of the upper layer.

In Section 2 our model is introduced. Section 2.1 presents the dimensional momentum, continuity and heat equations while Section 2.2 closes the system of equations by introducing the parameterization used for the entrainment velocity. In Section 2.3 the equations are non-dimensionalized. The DR's semigeostrophic model is

briefly reviewed and extended for our treatment of entrainment (Section 2.4). The finite difference scheme employed for the numerical calculations is sketched in Section 2.5. Section 3 presents and discusses the numerical solutions. In Section 4 the most relevant aspects of this work are summarized.

2. THE MODEL

2.1 Basic Equations

Consider a semi-infinite ocean of uniform depth consisting of two initially homogeneous constant depth layers bounded by a coast at x = 0. At time t = 0 we introduce the forcing effects of a constant wind stress in the alongshore direction, and heating. After this moment we will assume that all the variables will depend only on the cross-shelf direction. We eliminate surface oscillations by assuming a rigid lid, but otherwise the dynamical effect of the surface is obtained by introducing a surface pressure p_0 . The departure of the interface from its equilibrium position is given by η .

Let x and y be the cross-shelf and alongshelf directions respectively , x positive in the offshore direction, and let z be the vertical direction, positive upwards (Figure 1). Denote the velocity components in the x, y and z directions by u, v, w. The momentum and continuity equations for the two layers are

$$u_{1_t} + u_1 u_{1_x} - fv_1 = -\frac{1}{\rho_0} p_{1_x} + \frac{1}{\rho_0} \tau_z^x \qquad (1)$$

$$v_{1_t} + u_1 v_{1_x} + fu_1 = \frac{1}{\rho_0} \tau_z^y \qquad (2)$$

$$[(h_1-\eta)u_1]_x = \eta_t + w_e \qquad (3)$$

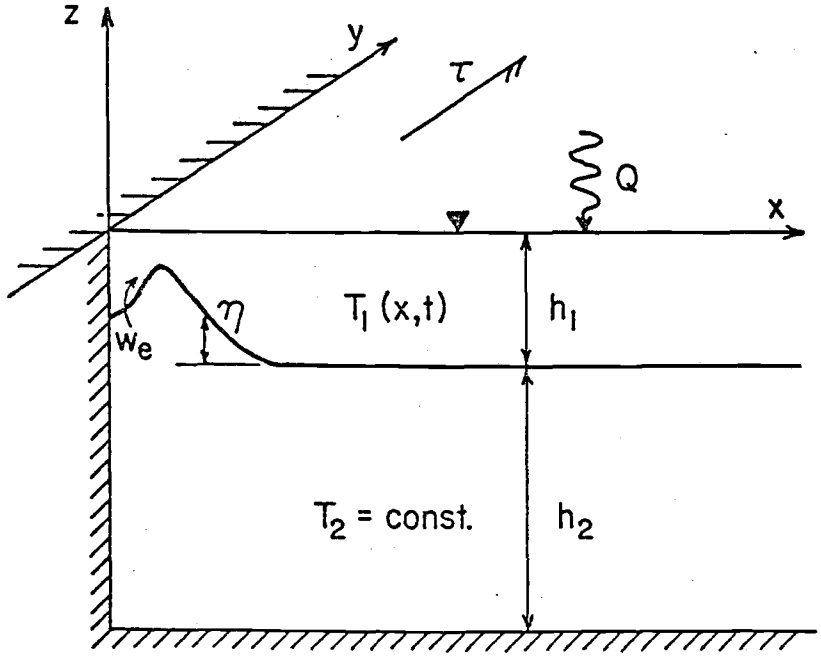

Figure 1

Schematic representation of the main elements of our model.

$$u_{2_t} + u_2 u_{2_x} - fv_2 = \frac{1}{\rho_0} p_{2_x} \tag{4}$$

$$v_{2_t} + u_2 v_{2_x} + fu_2 = 0 \tag{5}$$

$$[(h_2 + \eta)u_2]_x = -(\eta_t + w_e) \tag{6}$$

Subscripts 1 and 2 refer to the upper and lower layer respectively and differentiation is indicated by the letter subscripts. w_e is the entrainment velocity which represents the difference between the vertical velocity and the apparent motion of the interface (deSzoeke, 1980)

$$\begin{aligned} w_e &= w_1 - \frac{D\eta}{Dt} \\ &= (h_1 - \eta)u_{1_x} - (\eta_t + u_1 \eta_x) \\ &= [(h_1 - \eta)u_1]_x - \eta_t \end{aligned} \tag{3'}$$

which is the same equation as (3).

The stress (τ) divergence term in (1) and (2) can be written in linear form in virtue of the assumed vertical independence (deSzoeke, 1980)

$$\tau_z^y = \frac{\tau_0^y - \tau_e^y}{h_1 - \eta} \qquad \tau_z^x = \frac{-\tau_e^x}{h_1 - \eta} \tag{7}$$

where τ_0^y is the wind stress (by assumption in the y direction) and τ_e^x , τ_e^y are the interfacial entrainment stresses in the x and y directions. Following Niiler (1975) they can be expressed as

$$\tau_e^x = \rho(u_1 - u_2)w_e$$

$$\tau_e^y = \rho(v_1 - v_2)w_e \tag{8}$$

which represent the rate at which lower layer fluid is incorporated into the upper layer. The pressure in both layers is given by

$$p_1(x,t) = p_0(x,t) - g\rho_1 z$$

$$p_2(x,t) = p_0(x,t) - g(\rho_2 - \rho_1)(h_1 - \eta) - \rho_2 g z \tag{9}$$

where ρ_1 and η are functions of x and t, while ρ_2 is constant. The cross-shore pressure gradients are

$$p_{1_x}(x,t) = p_{0_x} - g\rho_{1_x} z \tag{10}$$

$$p_{2_x}(x,t) = p_{0_x} + g(h_1 - \eta)\rho_{1_x} + g(\rho_2 - \rho_1)\eta_x \tag{11}$$

In order to be consistent with our assumption of vertical independence we follow DR and substitute p_{1_x} by its vertical average over the upper layer

$$p_{1_x} = p_{0_x} + \tfrac{1}{2} g(h_1 - \eta)\rho_{1_x} \tag{10'}$$

As DR indicate this natural first approximation can be formally justified as corresponding to the lowest order coefficient in a vertical expansion in terms of orthogonal basis functions. Neglecting salinity effects we can write

$$\rho_2 - \rho_1 \equiv \Delta\rho = \rho_0\alpha\Delta T \equiv \rho_0\alpha(T_1 - T_2) \tag{12}$$

where α is the thermal expansion coefficient.

Equations (1) to (6) become

$$u_{1_t} + u_1 u_{1_x} - fv_1 = \frac{-1}{\rho_0} p_{0_x} + \frac{1}{2}\alpha g \Delta T_x (h_1 - \eta) - \frac{(u_1 - u_2)w_e}{h_1 - \eta} \tag{1'}$$

$$v_{1_t} + u_1 v_{1_x} + fu_1 = \frac{\tau^y_0}{\rho_0 (h_1 - \eta)} - \frac{(v_1 - v_2)w_e}{h_1 - \eta} \tag{2'}$$

$$[(h_1 - \eta)u_1]_x = \eta_t + w_e \tag{3'}$$

$$u_{2_t} + u_2 u_{2_x} - fv_2 = \frac{-1}{\rho_0} p_{0_x} + g(h_1 - \eta)\Delta T_x - g\alpha\Delta T\eta_x \tag{4'}$$

$$v_{2_t} + u_2 v_{2_x} + fu_2 = 0 \tag{5'}$$

$$[(h_2 + \eta)u_2]_x = -(\eta_t + w_e) \tag{6'}$$

The heat equation for the upper layer is

$$\frac{\partial T_1}{\partial t} + u_1\frac{\partial T_1}{\partial t} = -\frac{\partial}{\partial z}(\overline{w'T'})$$

$$= \frac{1}{(h_1-\eta)}[-\overline{w'T'}\Big|_0 + \overline{w'T'}\Big|_{h_1-\eta}]$$

$$= \frac{1}{(h_1-\eta)}[\frac{Q}{c\rho}_0 - \Delta T w_e] \qquad (13)$$

where $\overline{w'T'}$ is the turbulent vertical transport of heat,

Q is the surface heat flux,

and c is the specific heat of water at constant pressure.

We can obtain a conservative form for the system of equations (1')-(6') and (7) by multiplying (1)-(3) and (7) by the depth of the upper layer, $h_1-\eta$, and (4)-(6) by the depth of the lower layer, $h_2+\eta$. After some rearrangements we get

$$[(h_1-\eta)u_1]_t + [(h_1-\eta)u_1u_1]_x + f(h_1-\eta)v_1 =$$

$$-\frac{(h_1-\eta)}{\rho_0}p_{0_x} + \frac{g\alpha}{2}(h_1-\eta)^2\Delta T_x + u_2w_e \qquad (14)$$

$$[(h_1-\eta)v_1]_t + [(h_1-\eta)u_1v_1]_x + f(h_1-\eta)u_1 = \frac{\tau^y_0}{\rho_0} + v_2w_e \qquad (15)$$

$$(h_1-\eta)u_{1\,x} = \eta_t + w_e \qquad (16)$$

$$[(h_1-\eta)u_1]_t + [(h_2+\eta)u_2u_2]_x - f(h_2+\eta)v_2 = \tag{17}$$

$$- \frac{(h_2+\eta)}{\rho_0}p_{0_x} + g\alpha(h_1-\eta)(h_2+\eta)\Delta T_x - g\alpha\Delta T(h_2+\eta)\eta_x - w_e u_2$$

$$[(h_2+\eta)v_2]_t + [(h_2+\eta)u_2v_2]_x + f(h_2+\eta)u_2 = -w_e v_2 \tag{18}$$

$$[(h_2+\eta)v_2]_x = -(\eta_t + w_e) \tag{19}$$

$$[(h_1-\eta)\Delta T]_t + [u_1(h_1-\eta)\Delta T]_x = \frac{Q}{c\rho_0} \tag{20}$$

Define the following volume fluxes

$$U = (h_1 - \eta)u_1 = -(h_2 + \eta)u_2 \tag{21a}$$

$$V_1 = (h_1 - \eta)v_1 \tag{21b}$$

$$V_2 = (h_2 + \eta)v_2 \tag{21c}$$

where (21a) is satisfied because of (16) and (19). By substituting (21) into (14)-(20) we obtain

$$U_t + \left(\frac{U^2}{h_1-\eta}\right)_x - fV_1 = -\frac{(h_1-\eta)}{\rho_0}p_{0_x} + \frac{g\alpha}{2}(h_1-\eta)^2\Delta T_x - \frac{Uw_e}{h_2+\eta} \tag{14'}$$

$$V_{1_t} + \left(\frac{UV_1}{h_1-\eta}\right)_x + fU = \frac{\tau_0^y}{\rho_0} + \frac{V_2 w_e}{h_2+\eta} \tag{15'}$$

$$U_x = \eta_t + w_e \tag{16'}$$

$$- U_t + \left(\frac{U}{h_2+\eta}\right)_x - fV_2 = -\frac{(h_2+\eta)}{\rho_0}p_{0_x} + g(h_1-\eta)(h_2+\eta)\Delta T_x - g\alpha\Delta T(h_2+\eta)\eta_x - \frac{Uw_e}{h_2+\eta} \tag{17'}$$

$$V_{2_t} - \left(\frac{UV_2}{h_2+\eta}\right)_x - fU = \frac{-Uw_e}{h_2+\eta} \tag{18'}$$

$$[(h_1-\eta)\Delta T]_t + (U\Delta T)_x = \frac{Q}{c\rho_0} \tag{19'}$$

(14') and (17') can be added to give

$$\frac{p_{0_x}}{\rho_0} = \frac{f(V_1+V_2)}{H} - \left[\frac{U^2}{(h_1-\eta)(h_2+\eta)}\right]_x - \frac{g\alpha\Delta T}{H}(h_2+\eta)\eta_x + \frac{g\alpha(h_1-\eta)}{H}\left(h_2+\frac{h_1+\eta}{2}\right)\Delta T_x \tag{17''}$$

where $H=h_1+h_2$ is the total depth.

2.2 Entrainment Parameterization

To close the system the entrainment needs to be specified. Niiler and Kraus (1977) by vertically integrating the turbulent kinetic energy in its balanced form (d/dt=0) obtained the following approximate expression

$$w_e(Ri - s)\delta\underset{\sim}{v}^2 = 2mu_s^3 - \frac{\alpha g}{\rho c}(h_1-\eta)Q \tag{22}$$

where $\delta\underset{\sim}{v}^2=(v_1-v_2)^2$ and $\underset{\sim}{v}_1=(u_1,v_1)$, $\underset{\sim}{v}_2=(u_2,v_2)$,

$$Ri = g(\Delta\rho/\rho)(h_1-\eta)/\delta\underset{\sim}{v}^2 = \alpha g\Delta T(h_1-\eta)/\delta\underset{\sim}{v}^2 \tag{23}$$

is a local Richardson number,

$u_s=(\tau_0^y/\rho_0)^{\frac{1}{2}}$ is the surface friction velocity,

and s, m are parameters that need to be specified (see Niiler and Kraus, 1977, for their interpretation).

Price, et al. (1978) have suggested a value of 0.67 for s while Davis, et al. (1981) used 0.5 for m.

Equation (22) can be rewritten as

$$w_e = \frac{2}{\Delta T(1 - s/Ri)} \left[\frac{mu_s^3}{\alpha g(h_1-\eta)} - \frac{Q}{c\rho}\right] \tag{24}$$

Notice that for large Richardson numbers (23) becomes

$$w_e = \frac{2}{\Delta T} \left[\frac{mu_s^3}{\alpha g(h_1-\eta)} - \frac{Q}{c\rho}\right] \tag{25}$$

which is KT parameterization for the entrainment. On the other hand if either δv^2 becomes large or ΔT small then the Richardson number will approach a critical value s. In this case it becomes the dominant criterion for entrainment as propossed by PRT.

Equations (14') to (19') with either (23) or (24) constitute a closed system which can be solved numerically. Before doing so we proceed to non-dimensionalize the equations by using an adequate set of scales.

2.3 Scaling

Let the non-dimensional variables be momentarily primed. Following DR we introduce the following scaling

$$x = \lambda_* x' \qquad \lambda_*^2 = \frac{\alpha g T_* h_*}{f} = 2mu_s/f$$

$$
\begin{aligned}
t &= t_* t' & t_* &= \lambda_*/v_* = h_*/2mu_s \\
U &= h_* v_* u' & v_* &= u_s^2/(fh_*) \\
(V_1, V_2) &= h_* v_* (V_1', V_2') & & \qquad (26) \\
p_0 &= p_* p_0' & p_* &= \rho_0 f v_* \lambda_* = \rho_0 v_*^2 q \\
\eta &= h_* \eta' & h_* &= mu_s^3 \Big/ \left(\frac{\alpha g Q_*}{2c\rho_0}\right) \\
w_e &= w_* w_e' & w_* &= h_* v_*/\lambda_* \\
T &= T_* \Delta' & T_* &= \lambda_* \left(\frac{Q_*}{c\rho_0}\right)\left(\frac{f}{u_s^2}\right) \\
Q &= Q_* Q' & &= \frac{2mQ_*}{\rho_0 c u_s} \\
\tau_0^y &= \tau_* \tau' & \tau_* &= \rho_0 u_s^2
\end{aligned}
$$

h_* is the Monin-Obukhov depth; in the KT parameterization it establishes an upper limit for the depth of the mixed layer, corresponding to a zero net entrainment velocity. T_* is obtained by making the time dependent and advective heat fluxes comparable to the surface heat flux. λ_* is the Rossby radius of deformation based on the upper layer depth scale and the temperature scales. t_* is obtained by making the local rate of change and horizontal advection of momentum comparable; it can also be obtained from the continuity equation by comparing the velocity divergence with the rising of the interface. v_* is an Ekman velocity for an upper layer with depth h_* ; although it is representative only for the cross-shelf

direction its choice for both components facilitates the study of the inertial oscillations. w_* can be obtained through the continuity equation. p_* is chosen such that it makes the surface pressure gradient comparable to the Coriolis term in the cross-shore momentum equation. Table 1 shows the values taken by these scales for typical driving functions.

With this scaling, equations (14') to (19') (with (17'') instead of (17')) and (24) become (dropping primes)

$$U_t + \left(\frac{U^2}{h_i-\eta}\right)_x - qV_1 = -q(h_i-\eta)p_{0_x} + \frac{q^2}{2}(h_i-\eta)\Delta_x - \frac{\gamma U w_e}{1-\gamma h_i+\gamma\eta} \tag{27}$$

$$V_{1_t} + \left(\frac{UV_1}{h_i-\eta}\right)_x + qU = q\tau + \frac{\gamma V_2 w_e}{1-\gamma h_i+\gamma\eta} \tag{28}$$

$$U_x = \eta_t + w_e \tag{29}$$

$$p_{0_x} = \gamma(V_1+V_2) - \frac{1}{q}\left[\frac{\gamma U^2}{(h_i-\eta)(1-\gamma h_i+\gamma\eta)}\right]_x - q[(1-\gamma h_i+\gamma\eta)\Delta\eta_x - (h_i-\eta)(2-\gamma h_i+\gamma\eta)\Delta_x/2] \tag{30}$$

$$V_{2_t} - \left(\frac{\gamma UV_2}{1-\gamma h_i+\gamma\eta}\right)_x - qU = \frac{-\gamma V_2 w_e}{1-\gamma h_i+\gamma\eta} \tag{31}$$

$$[(h_i-\eta)\Delta]_t + (U\Delta)_x = Q \tag{32}$$

$$w_e = \frac{\tau^{3/2}/(h_i-\eta) - Q}{[1 - s/(q^2Ri)]} \tag{33}$$

Table 1

Characterization of the variables and parameters appearing in our model. The driving functions and parameters employed are the following:

$\tau = \rho u_s^2 = 0.1$ Pa , $Q = 75$ W/m^2,

$\alpha = 1.7 \times 10^{-4}$ C^{-1}, $g = 9.8$ m/s^2, $c = 4.1 \times 10^3$ J/(kg C),

$\rho = 10$ kg/m^3, $f = 10^{-4}$ s^{-1}, $m = 0.5$ (Davis, et al, 1981).

Table 1

Variable	Scale	Typical Value
Temperature difference, Δ	$T_* = \lambda_* \frac{Q_* f}{\rho c u_s^2}$ $= 2mQ_*/(\rho c u_s)$	1.8×10^3 C
Interface elevation, η	$h_* = \frac{2mu_s^3}{(\alpha g Q_*/c\rho)}$	33 m
Horizontal distance, x	$\lambda_* = (g\alpha T_* h_*)^{\frac{1}{2}}/f$ $= 2mu_s/f$	100 m
Time, t	$t_* = \lambda_*/v_* = h_*/(2mu_s)$	3300 s
Horizontal velocities, u_1, u_2, v_1, v_2	$v_* = u_s^2/(fh_*)$	3 cm/s
Entrainment velocity, w_e	$w_* = h_* v_*/\lambda_*$	1 cm/s

Parameters

Aspect ratio,	$\gamma = h_*/H = 0.1$	H=330 m
Initial depth,	$h_i = h_1/h_* = 0.5$	h_1=16.5 m
Initial temperature difference,	$\Delta_i = \Delta T_i/T_* = 180$ [1000]	ΔT_i=0.32 °C [1.8 °C]
Non-dimensional inertial frequency,	$q = ft_* = 4m\ h_*/\lambda_*$ $= 0.33$	

For large Richardson numbers (33) reduces to the KT parameterization

$$w_e = \frac{\tau^3 2 - Q(h_i - \eta)}{\Delta(h_i - \eta)} \qquad (33')$$

The non-dimensional velocities in the upper and lower layer can be easily recovered from

$$u_1 = \frac{U}{h_i - \eta} \qquad u_2 = \frac{-\gamma U}{1 - \gamma h_i + \gamma \eta}$$
$$v_1 = \frac{V_1}{h_i - \eta} \qquad v_2 = \frac{\gamma V_2}{1 - \gamma h_i + \gamma \eta} \qquad (34)$$

The four parameters appearing in the equations are

$\gamma = h_*/H$, the ratio of the upper layer depth scale to the total depth.

$h_i = h_1/h_*$, which is a measure of the initial depth of the upper layer.

$\Delta_i = \Delta T_i/T_*$, which gives the initial temperature difference between both layers in units of T_*.

$q = ft_*$, is a non-dimensional inertial frequency. It can be rewritten as $q = (\alpha g h_* T_*/v_*^2) = 4m^2 h_*/\lambda_*$ which shows that it also corresponds to the square root of a Richardson number formed with our scaling for the problem. The true non-dimensional Richardson number, Ri, which arises from the dimensional quantities, can be expressed as

$$Ri = q^2 Ri_* \qquad (35a)$$

where

$$Ri_* = \frac{(h_i-\eta)\Delta}{(u_1-u_2)^2+(v_1-v_2)^2} \tag{35b}$$

is calculated using the non-dimensional variables.

For given values of the driving functions τ , Q and a particular choice of the Coriolis frequency f, the scales T_* , h_* and the parameter q become totally specified. Hence, different initial conditions can be set through h_i and Δ_i . Some characteristic values for these parameters are shown in Table 1.

An estimate for the time that takes for the front to upwell (upwelling time) is given by $t_0=\lambda_i/u_0$, where $u_0=u_s^2/fh_1$ is the Ekman velocity and $\lambda_i=(\alpha g\Delta T_i h_1)^{\frac{1}{2}}/f$ is the initial Rossby radius of deformation. t_0 can be related to our time scale t_* by $t_0=(\Delta_i h_i^3)^{\frac{1}{2}}t_*$ which shows that the thermocline will upwell at non-dimensional times approximately equal to $(\Delta_i h_i^3)^{\frac{1}{2}}$ (actually earlier due to entrainment).

RA have discussed the physical meaning of a parameter given by

$$q_0 = \frac{\alpha g\Delta T_i h_1}{u_0^2} = (ft_0)^2 \tag{36}$$

which can be related to q by $q_0=q^2(\Delta_i h_i^3)^{\frac{1}{2}}$. They show how as q_0 becomes large the full momentum equations

approximate to the semigeostrophic solution. Hence, in our scaling we would require $q^2(\Delta_i h_i^3)^{\frac{1}{2}}$ to become large (of the order of 1000 or more) for our solution to approach the semigeostrophic limit.

2.4 Semigeostrophic Approximation

It could be argued that near the coast either the length or the velocity scale in the alongshore direction are large compared with those in the cross-shore direction, and that the terms $u_{1_t}+u_1u_{1_x}$ and $u_{2_t}+u_2u_{2_x}$ in equations (1) and (4) are small compared to the Coriolis force associated with the alongshore velocity. This is the so called semigeostrophic approximation (Pedlosky, 1979, page 404) and it was employed by DR. It has the advantage of reducing the complexity of the system and permits the elegant semi-analytical treatment followed by DR. However, the elimination of the time-dependent terms totally filters the inertial oscillations which are very important far offshore, and, during the process of adjustment after a wind set-up, are responsible for behaviour very different from the semigeostrophic case. In particular, the neglect of these terms sets up an offshore Ekman balance in an infinitesimal time. As mentioned in the introduction the other possible important role of the inertial oscillations is to enhance the shear mixing mechanism. In order to look into the accuracy of

these statements DR's model has been extended to calculate the upper layer alongshore velocity. Also, this will permit us to calculate the shear at the interface and to use equation (23) for the entrainment velocity.

The semigeostrophic non-dimensional system is

$$v_1 = p_{0_x} - \tfrac{1}{2}h\Delta_x + \frac{1}{q}\frac{(u_1-u_2)w_e}{h_1} \tag{37}$$

$$v_{1_t} + u_1 v_{1_x} + qu_1 = q\tau/h - \frac{w_e(v_1-v_2)}{h} \tag{38}$$

$$h_t + (hu_1)_x = w_e \tag{39}$$

$$v_2 = p_{0_x} - h\Delta_x - \Delta h_x \tag{40}$$

$$v_{2_t} + u_2 v_{2_x} + qu_2 = 0 \tag{41}$$

$$(h\Delta)_t + (h\Delta u_1)_x = Q \tag{42}$$

where $h \equiv (h_i - \eta)$ is introduced to maintain the notation close to DR. For comparison with DR notice that we have set the bottom Ekman velocity to zero. DR manipulated this system to obtain

$$\frac{d}{dt}(h\Delta) = -u_{1_x}\Delta + Q \tag{43}$$

$$\frac{d}{dt}h = -u_{1_x}h_1 + w_e \tag{44}$$

$$\frac{d}{dt}P = P\frac{\gamma w_e}{1-\gamma h} \tag{45}$$

$$-(h_1{}^2\Delta u_{1_x})_x + hPu_1 = \tau \tag{46}$$

P is the lower layer potential vorticity,

$$P = \gamma \frac{(1+v_{2_x}/q)}{1-\gamma h} \tag{47}$$

which is scaled by $P_* = f/H$. The d/dt derivatives are following the characteristics, i.e.

$$\frac{dx_1}{dt} = u_1 \quad , \qquad x_1(0,\xi) = \xi \tag{48}$$

$$\frac{dx_2}{dt} = u_2 \quad , \qquad x_2(0,\xi) = \xi \tag{49}$$

DR calculated the lower layer alongshore velocity as

$$v_2(x,t) = q \int_0^x [(1-h/\gamma)P-1]dx \tag{50}$$

The upper layer alongshore velocity can be obtained by solving

$$\frac{d}{dt} v_1 = -qu_1 + q\tau/h - \frac{w_e(v_1-v_2)}{h} \tag{51}$$

where d/dt is along the characteristic (48). The entrainment velocity is given by equation (33).

2.5 Numerical Analysis

The non-dimensional system of equations (27)-(33) is approximated by its finite difference representation (see Appendix A). The initial condition at all points is a

state of rest, i.e all volume fluxes, interface elevation and surface pressure gradient are set to zero, and the temperature difference is set to its full value, Δ_i . The boundary conditions are of no flux normal to the shore , ie. $U = 0$ at $x = 0$, and a smooth transition for all variables at large values of x ($\partial U/\partial x = 0$). For this last condition to be true we require a spatial grid large enough that the gradients of all variables at its offshore extreme are always small, ie. such that for the largest time considered the front has not had time to cross the whole grid. The space discretization is small near the coast and the evolving front and larger further offshore; it has been chosen such that it can adequately resolve the fine details of the evolution. The time step has been chosen such that it satisfies both the Courant-Friedrich-Levy (or CFL) condition and a condition arising from the von Neumann stability analysis of the system of equations (see Appendix B). For all the cases studied the second condition dominates.

3. DISCUSSION

Comparison of the numerical results for several cases will serve our objectives. For brevity let's refer to the DR model , modified with the shear enhanced entrainment formulation, as DRM, and to our finite difference model, which includes inertial oscillations, as TLWE. The KT entrainment parameterization (wind as the source for turbulent kinetic energy) is given by equation (33'), which can be obtained from equation (33) by simply setting s = 0. The shear mechanism (PRT) can be included by setting s to a critical Richardson number; following Price et al (1978) we will use s = 0.67. First, DRM for s = 0 can be compared to TLWE for s = 0 in order to study the role of inertial oscillations in altering the divergence at the coast. Two values for the initial temperature difference between both layers will be used, specifically Δ_i = 180 and Δ_i = 1000. Second, the importance of the shear mixing mechanism can be assessed by comparing TLWE runs for s = 0 (KT) and s = 0.67 (KT and PRT). Finally, the effects of the alongshore coastal jet and the inertial oscillations can be isolated by considering DRM (which contains only the jet) for s = 0 and s = 0.67, and TLWE (which includes both the jet and inertial oscillations) for s = 0.67. Table 2 summarizes the conditions for the numerical results to be compared.

Run	Model	Δ_i	s
1	DRM	180	0.0
2	TLWE	180	0.0
3	DRM	1000	0.0
4	TLWE	1000	0.0
5	DRM	180	0.67
6	TLWE	180	0.67

Table 2

Summary of numerical runs. DRM refers to the DR model modified to allow for shear enhanced entrainment (Section 2.4). TLWE refers to the model described in this paper which includes inertial oscillations (Section 2).

The values employed for the parameters are those given in Table 1.

In the discussion to follow we will always refer to the non-dimensional quantities, but their corresponding dimensional values will be included within parenthesis. Notice that both $\Delta_i = 180$ (0.32 C) and $\Delta_i = 1000$ (1.8 C) correspond to relatively weak initial temperature stratification, and will produce only relatively weak fronts. They have been chosen because the minimum time step for the numerical scheme to be stable is given by $\min \Delta x / 2q(h_i(1-\gamma h_i)\Delta_i)^{\frac{1}{2}}$ (see Appendix B). However, these values already show all the frontal features. Furthermore, their associated q_0 (see Section 2.3), 2.5 and 13.6 respectively, are representative of two very different situations. The first value, $q_0 = 2.5$ corresponds to an upwelling time t_0 of 4.74 (4.35 h), while the second one, $q_0 = 13.6$, gives an upwelling time of $t_0 = 11.18$ (10.25 h). These values can be compared with the time of occurrence of the maximum offshore volume fluxes for the linear wind-driven problem (see equations (52) below), $t = \pi/q = 3\pi = 9.42$ (4.32 h). This shows that in the first case the thermocline will upwell before the maximum offshore fluxes and in the second case it will upwell afterwards. Notice that in the presence of entrainment the interface will never upwell (w_e goes to infinity as h goes to zero). In this case the

upwelling time can be obtained from the time that takes for entrainment to dominate over the horizontal volume flux divergence (η_t changes sign) and it will be less than u_0/λ_i .

Results for the DR model with $\Delta_i = 180$ and $s = 0$ are shown in Figure 2. In it the temperature difference between both layers, Δ , the lower layer potential vorticity, P, the upper layer depth, $h = h_i - \eta$, and the alongshore and cross-shore velocities, u_1 and v_1 , are displayed over the coastal region for different stages during upwelling. These results are essentially the same as those reported by DR with the exception that v_1 is now calculated. They show the inmediate establishment of an offshore Ekman balance (Figure 2a), the upwelling of the thermocline at about t = 3.3 (3.03 h) (Figure 2b) and the development and offshore propagation of a sharp front moving with the velocity of the upper layer (Figures 2c to 2f). The region onshore of the front (interior region) is decoupled from the region offshore from the front (exterior region). The alongshore velocity profiles show the formation of an increasingly strong baroclinic jet over the front itself, or frontal region (see, for example, Figure 2f at x = 10 (1 km)). This jet, occurring in a region of large density gradients, contrasts with the barotropic jet which develops near the coast during later stages (see Figure 2f for x = 3 (300 m)). If we calculate

Figure 2

Temperature difference, Δ, lower layer potential vorticity, P, upper layer cross-shore and alongshore velocities, u and v, and upper layer depth, h, obtained using the DRM model with $\Delta_i = 180$ and $s = 0$. The times for the sequence shown are: 2a, 0.95 (0.87 h); 2b, 3.3 (3.03 h); 2c, 3.8 (3.48 h); 2d, 4.3 (3.94 h); 2e, 5.7 (5.23 h); 2f, 9.0 (8.25 h).

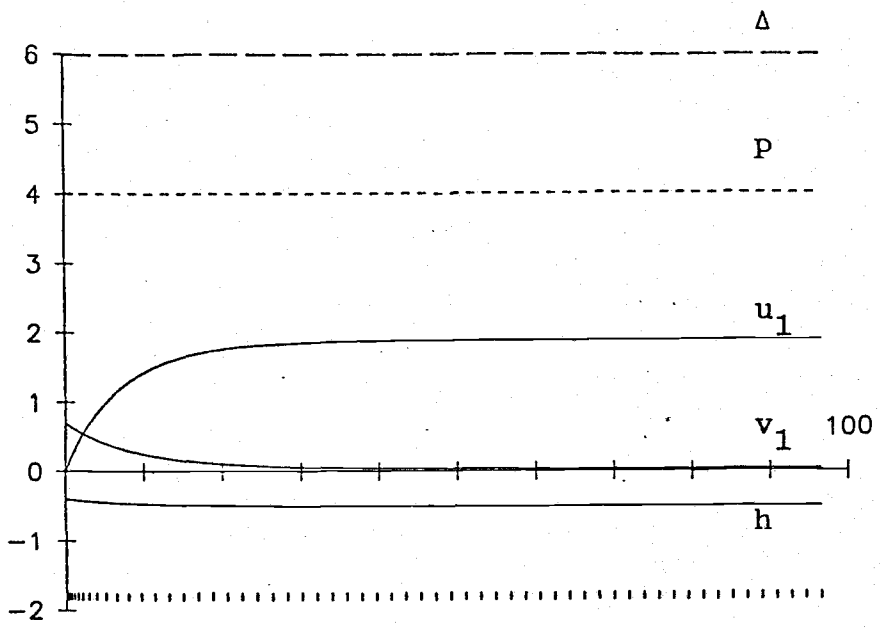

2a

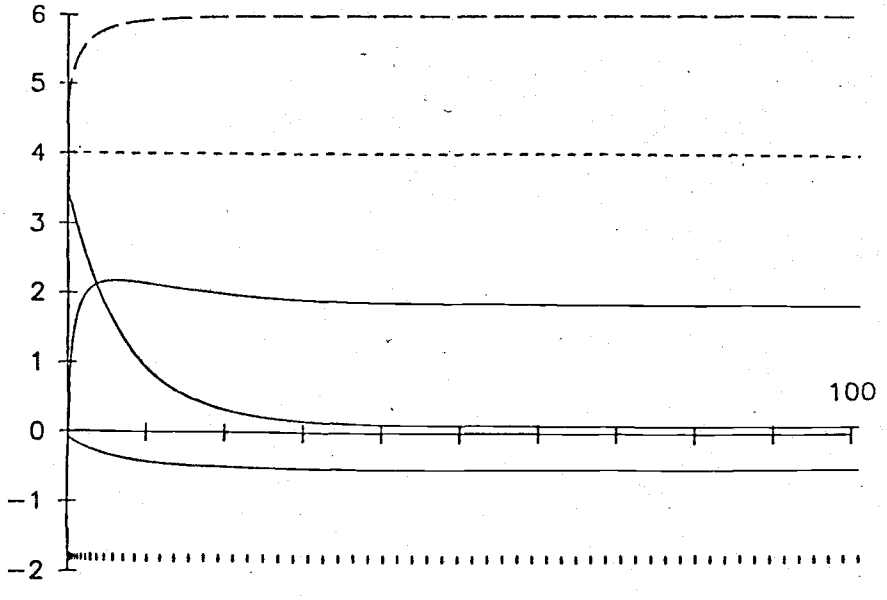

2b

Figure 2

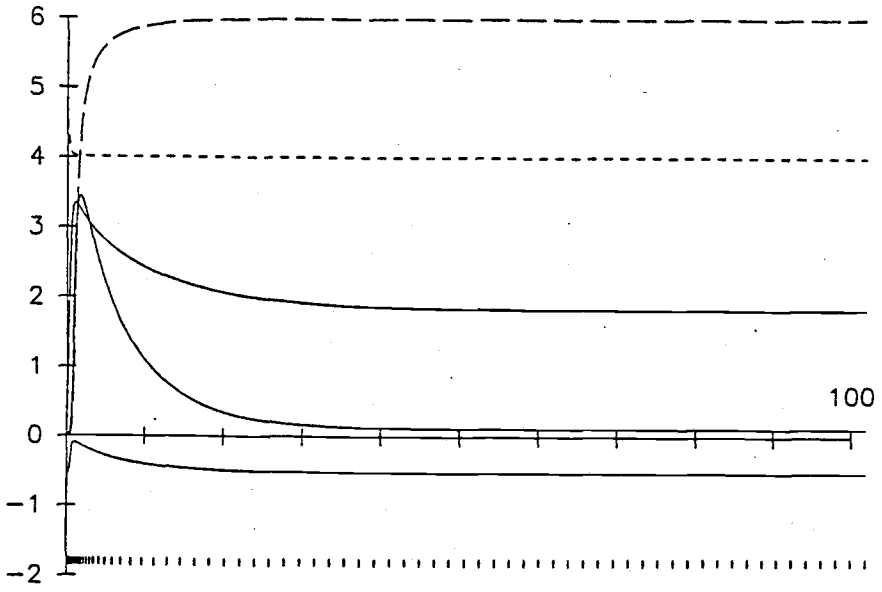

2c

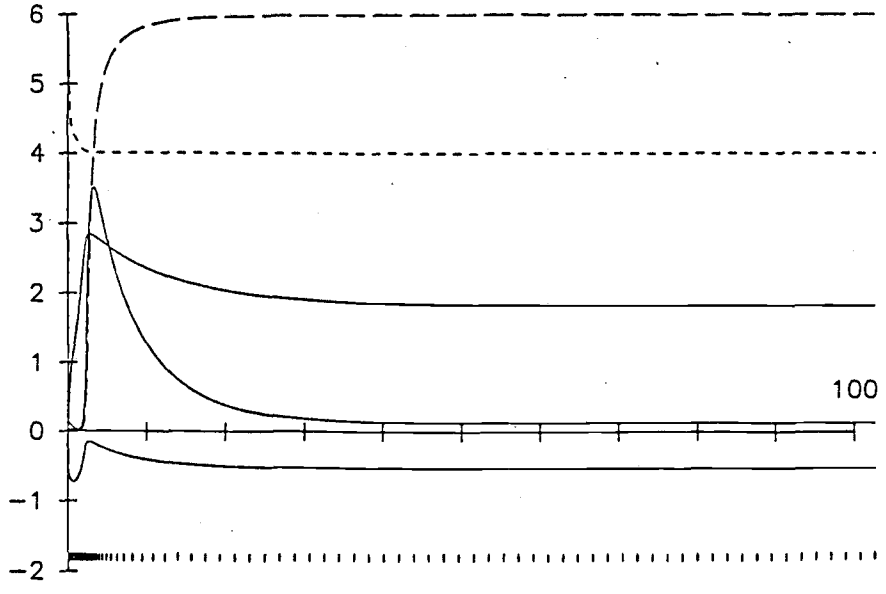

2d

Figure 2 (continued)

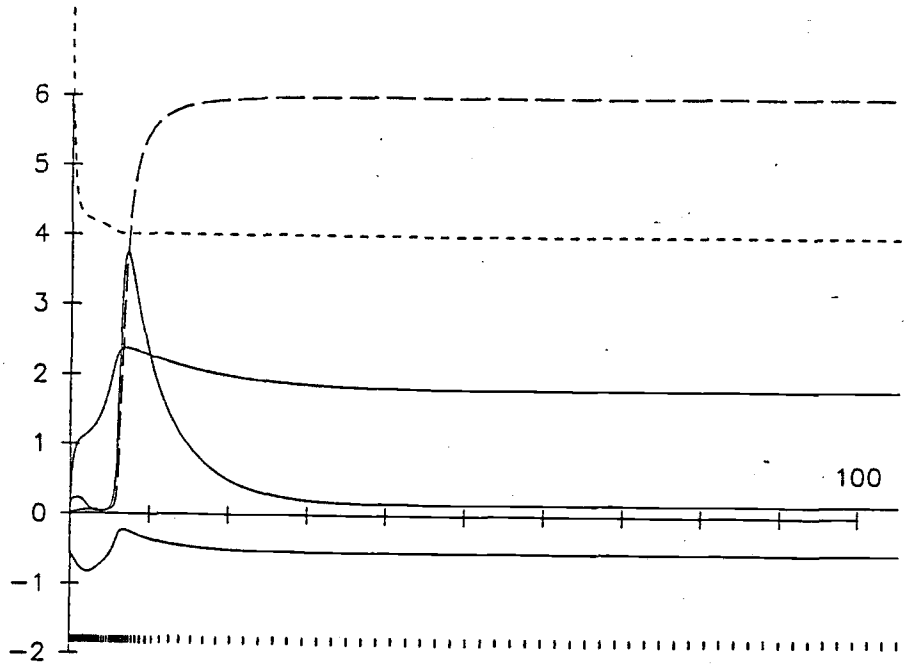

2e

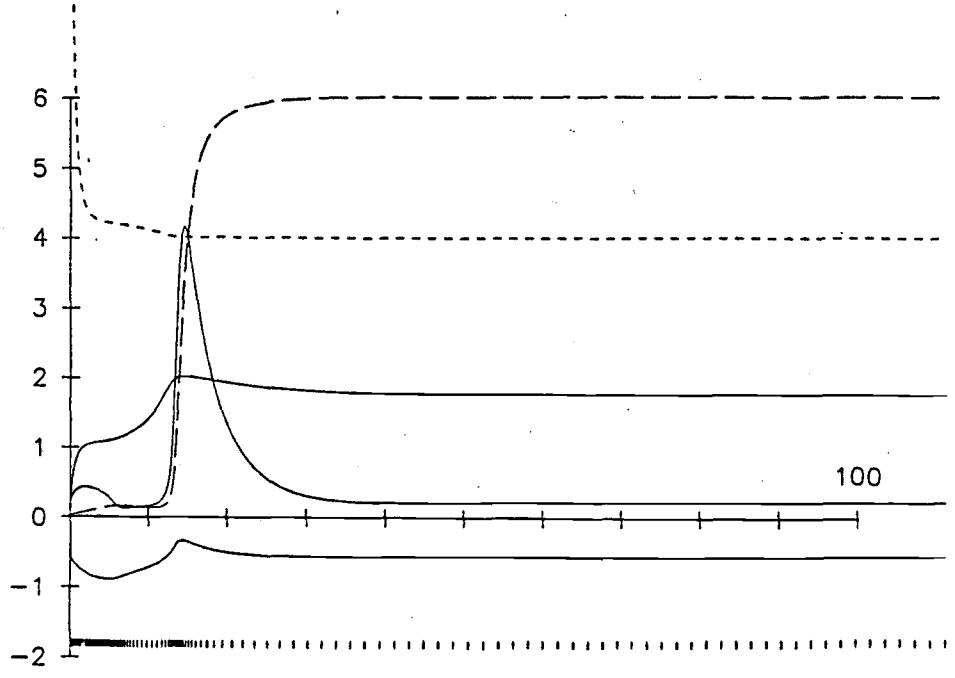

2f

Figure 2 (continued)

the offshore volume flux ($U = u_1 h$) it will be apparent that it goes from nearly its full value at a distance to zero at the coast. This distance is what we will call the length of adjustment, or Rossby radius of deformation. Its initial value is given by $\lambda_i = (h_i \Delta_i)^{\frac{1}{2}} = 9.5$, and gets progressively shorter until it becomes of the order of the horizontal length scale, λ_* (see DR). Simultaneously, the temperature near the coast changes from its full value $\Delta_i = 180$ (0.32 C) to the small value given by the temperature scale $\Delta = 1$ (0.0018 C) after the front has developed (Figures 2a and 2d). Notice, finally, how the interior region does not feel the exterior region, and instead tends towards a steady state solution as the one described by deSzoeke and Richman (1981).

Figure 3 corresponds to a run of the model TLWE with $s = 0$ and $\Delta_i = 180$. In it Δ , η , the entrainment velocity, w_e , and the cross-shore and alongshore volume fluxes, U and V_1 , are shown over the coastal region at different times during upwelling. Notice the slow development of the velocity offshore from a state of rest towards an Ekman balance with inertial oscillations. The presence of the inertial oscillations in the exterior region drives the divergence at the coast (Figure 3b) until the thermocline surfaces at about $t = 6.6$ (6.05 h) (Figure 3c). During this stage the length of adjustment

Figure 3

Temperature difference, Δ , interface elevation, η , entrainment velocity, w_e, and upper layer cross-shore and alongshore volume fluxes, U and V_1, obtained using the TLWE model with $\Delta_i = 180$ and s =0. The times for the sequence shown are: 3a, 1.0 (0.92 h); 3b, 4.0 (3.67 h); 3c, 7.0 (6.42 h); 3d, 9.0 (8.25 h); 3e, 11.0 (10.08 h); 3f, 14.0 (12.83 h).

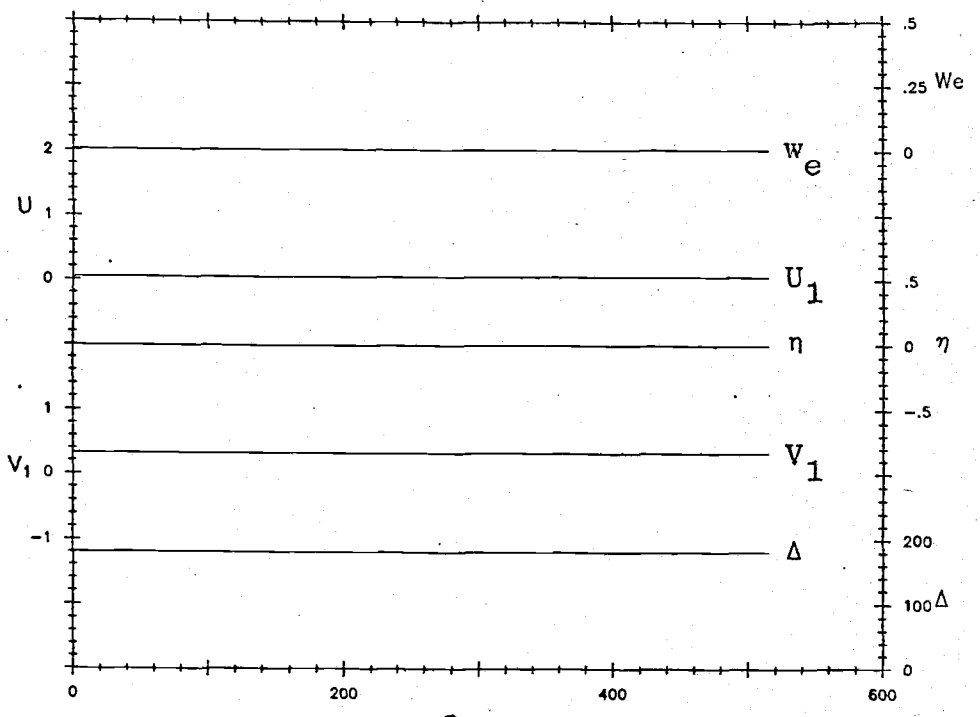

3a

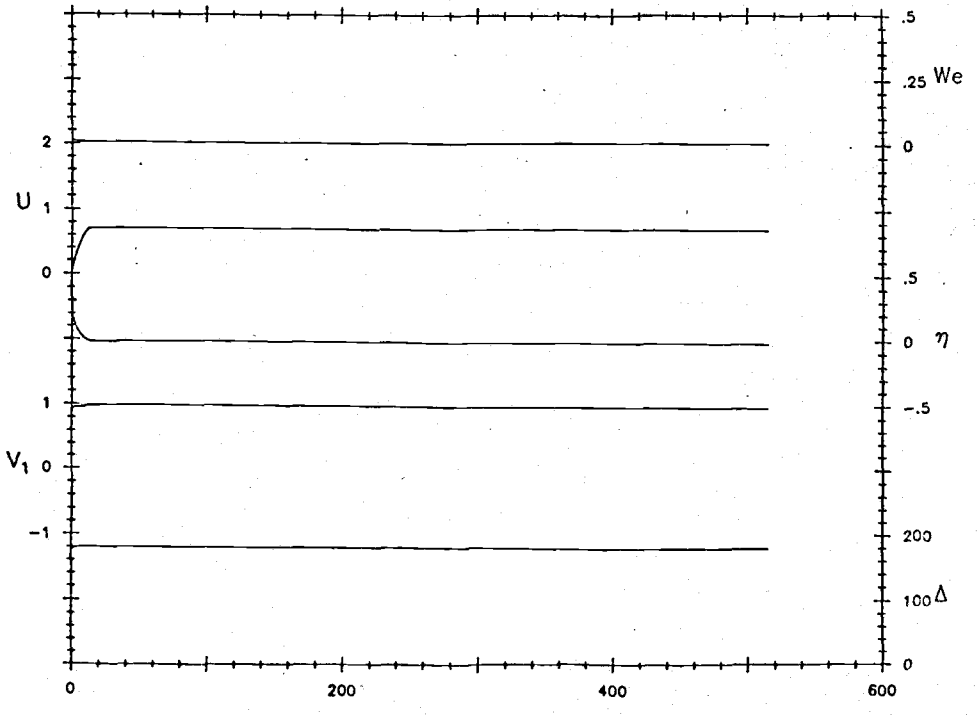

3b

Figure 3

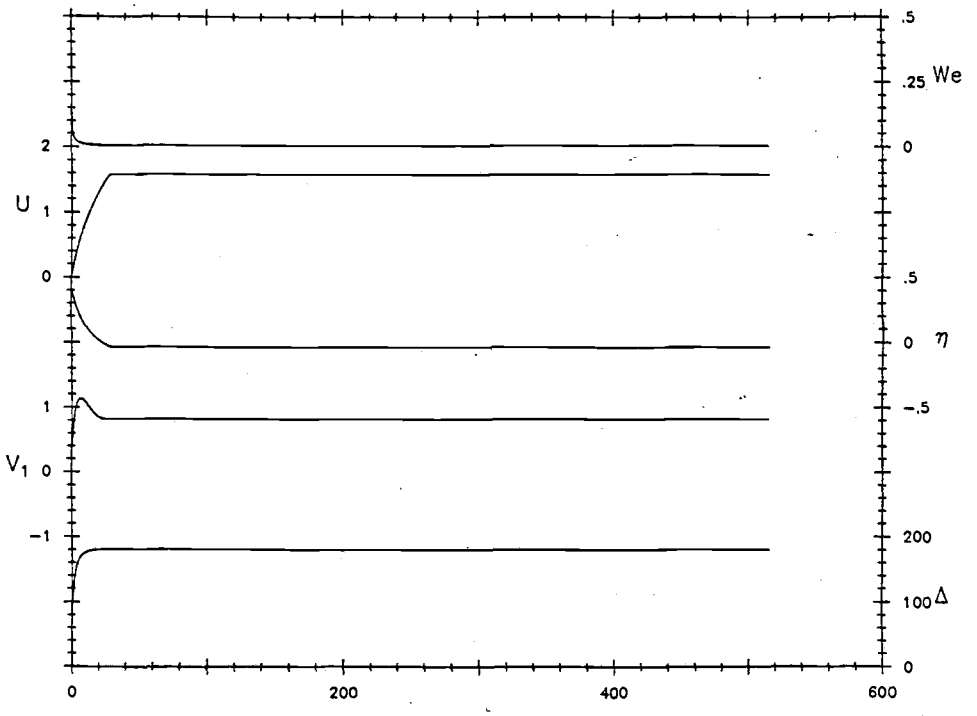

3c

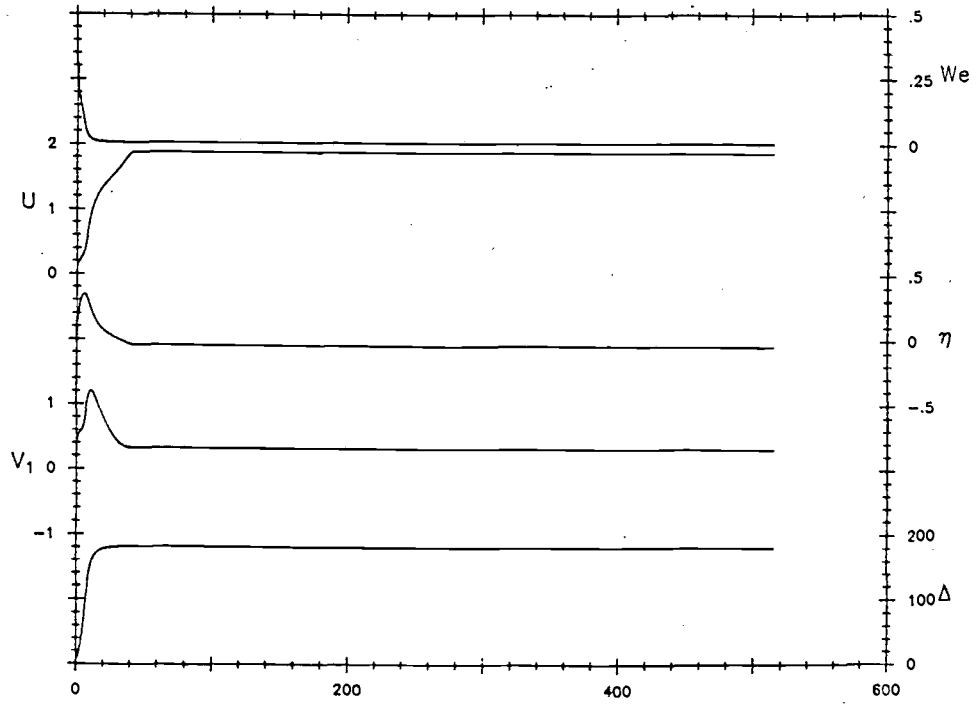

3d

Figure 3 (continued)

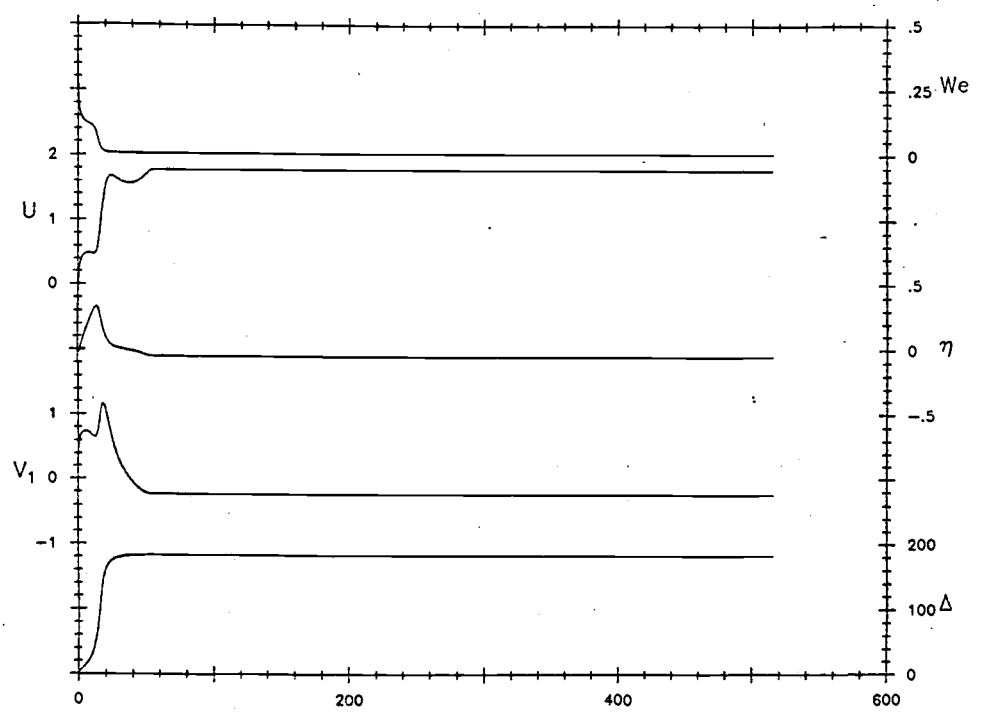

3e

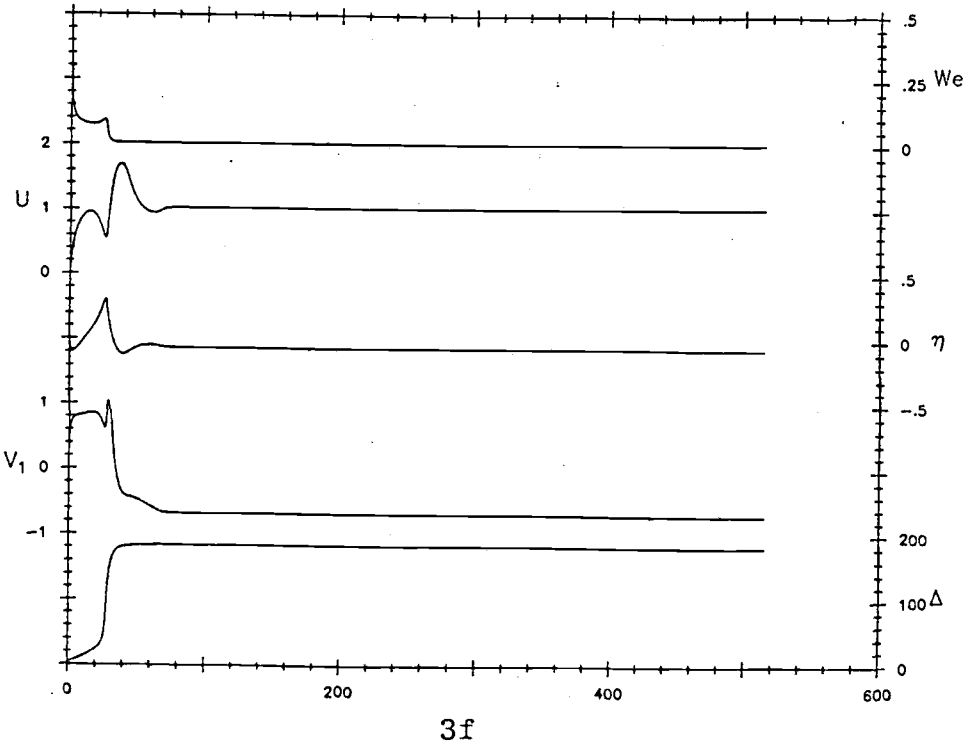

3f

Figure 3 (continued)

(corresponding to the area where the horizontal volume flux divergence occurs) increases until its full value is reached at about t = 9.5 (8.71 h) (Figure 3d). This acts to raise the interface and to enhance w_e over a larger area, which broadens the frontal region. The interior region, formed after the development of the front, is ignorant of the offshore oscillating regime , i.e. it is decoupled from the exterior region. When the cross-shore volume flux in the exterior region decreases considerably (the volume flux at the frontal region being unable to follow it; see Figure 3e) the horizontal volume flux divergence at the front becomes negative and forces the front to steepen like a shock wave (Figure 3d). This same case can be observed with more detail in Figure 4 which shows a smaller region near the coast; in it the upper layer cross-shelf and along-shelf velocities, u_1 and v_1, are shown. The decoupling between the interior region (large entrainment , nearly homogeneous in the vertical) and the exterior region (inertially dominated; no large stratification) is clear in the sequence shown, particularly in Figures 4d to 4f. Notice that in this case the interior region shows the offshore progression of a steady state solution. In particular, the curves for u_1, v_1 and h in the interior region are nearly the same at all times.

Figure 4

Temperature difference, Δ , interface elevation, η , entrainment velocity, w_e, and upper layer cross-shore and alongshore velocities, u_1 and v_1, for an expanded region near the coast, obtained using the TLWE model with Δ_i = 180 and s = 0. The times for the sequence shown are: 4a, 4.0 (3.67 h); 4b, 7.0 (6.42 h); 4c, 9.0 (8.25 h); 4d, 11.0 (10.08 h); 4e, 14.0 (12.83 h); 4f, 16.0 (14.67 h).

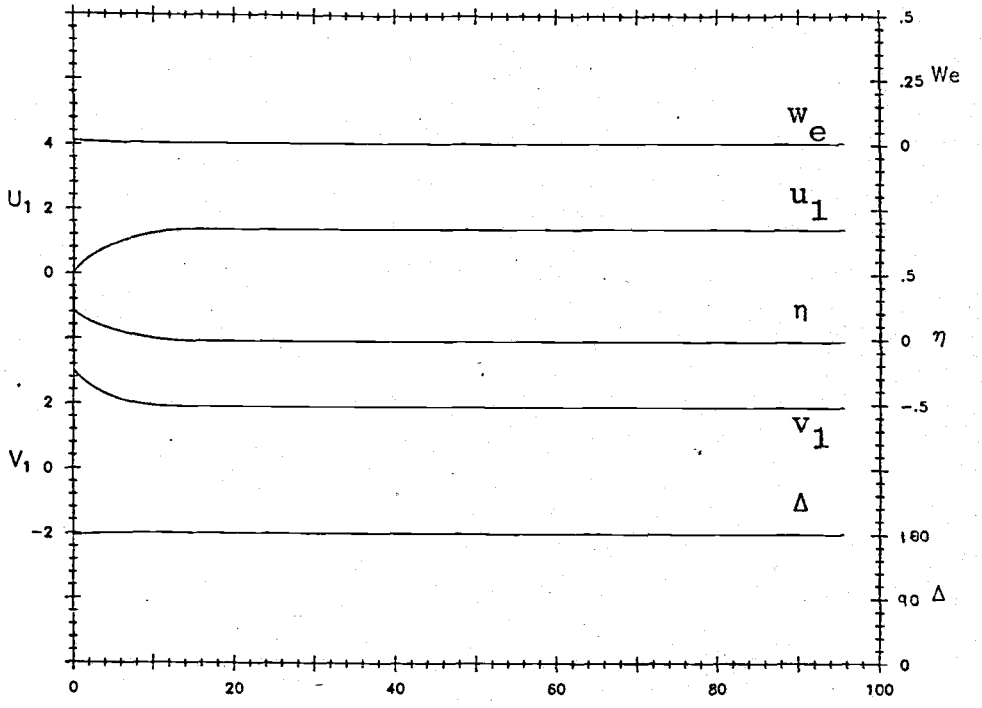

4a

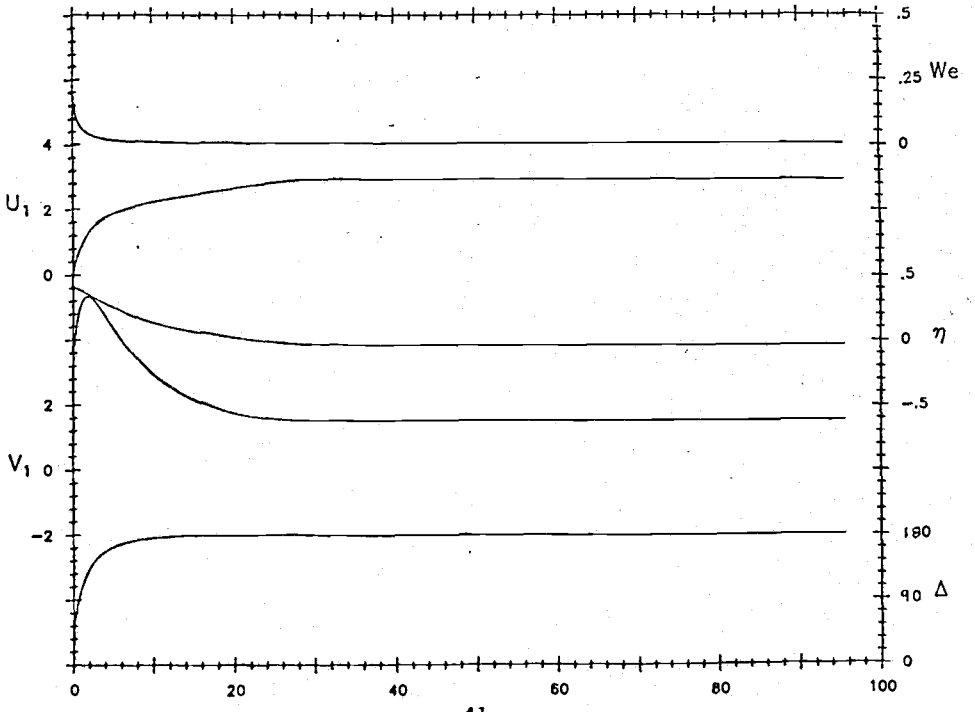

4b

Figure 4

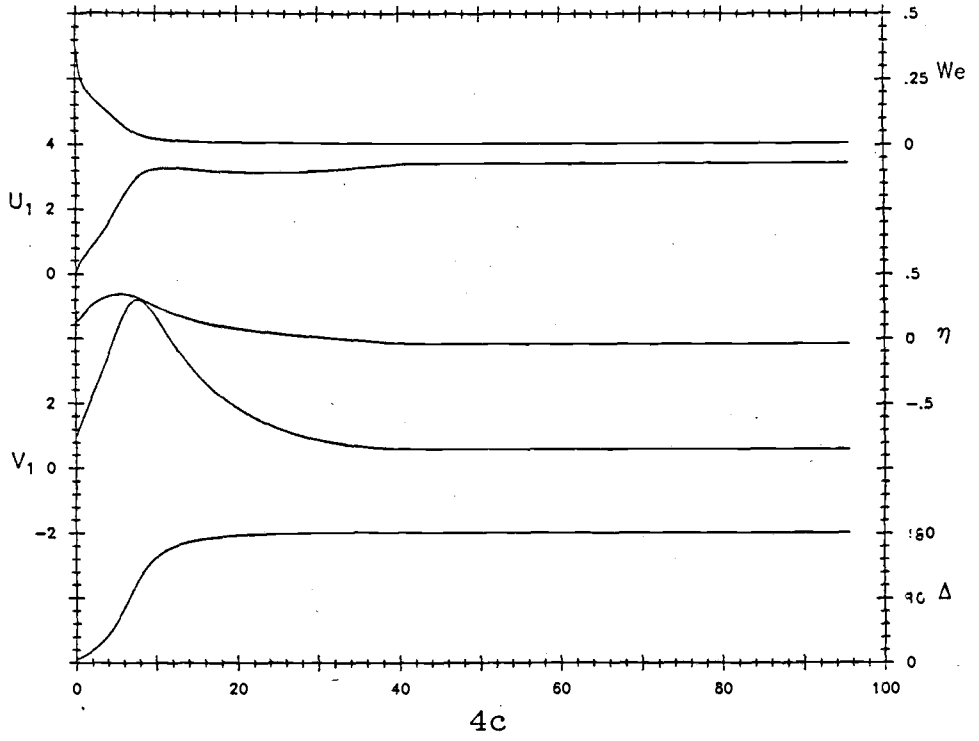

4c

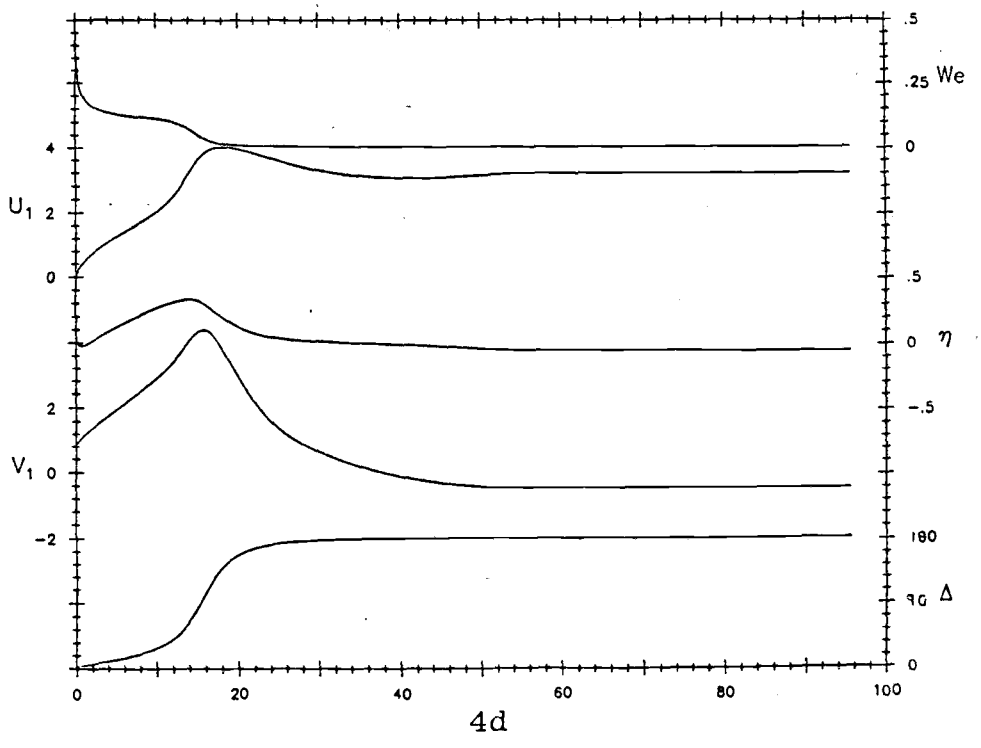

4d

Figure 4 (continued)

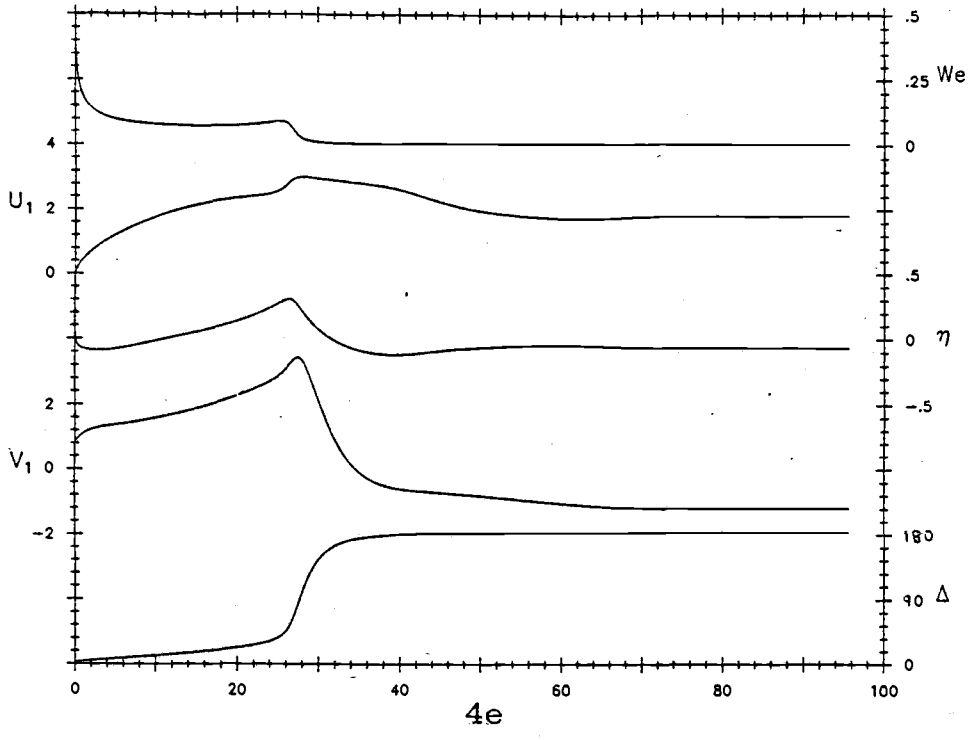

4e

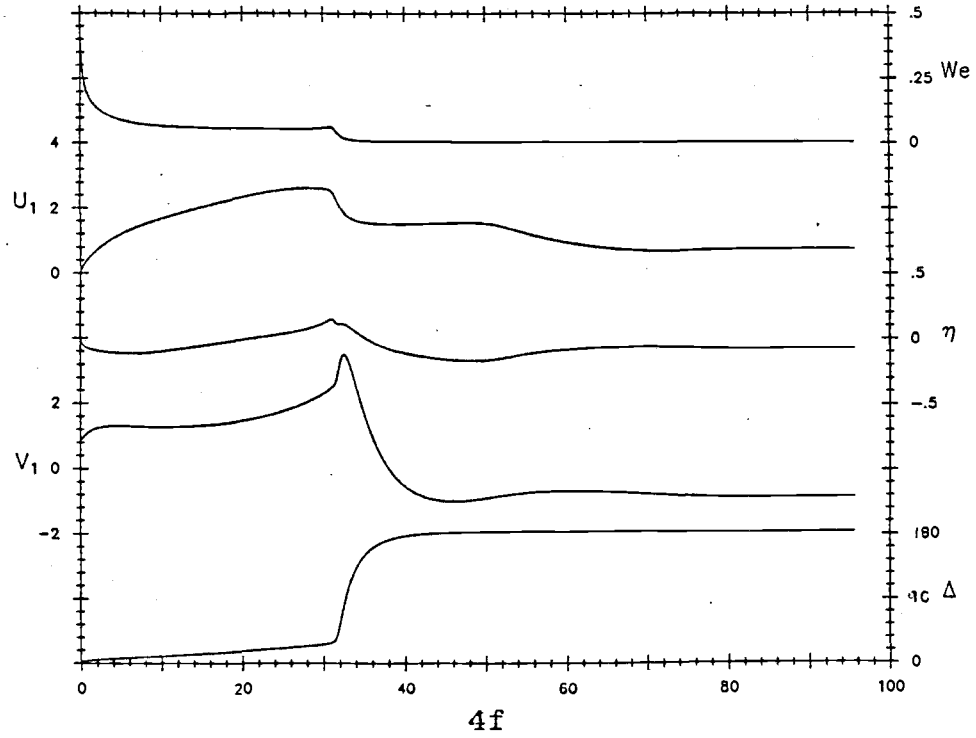

4f

Figure 4 (continued)

In Figure 5 is shown the numerical run for the DRM model with $s = 0$ and $\Delta_i = 1000$, while Figures 6 and 7 correspond to the results for TLWE with $s = 0$ and $\Delta_i = 1000$. The differences between them are similar to those described above. However, the increase in Δ_i has the following effects. 1) The length of adjustment is increased ($\lambda \propto \Delta_i$). Compare, for example, the situation at the time of surfacing of the thermocline: Figures 2b and 5a that for the DRM model λ has increased from about 5 to 10 (0.5 to 1 km), while Figures 3c and 6b show that for the TLWE model it has increased from 30 to nearly 100 (9 to 30 km). 2) The surfacing of the thermocline is delayed (it takes longer for For the DRM model the upwelling time increases from 3.4 (3.12 h) for $\Delta_i = 180$ to 8.0 (7.33 h) for $\Delta_i = 1000$; for the TLWE model it increases from 8.0 (7.33 h) for $\Delta_i = 180$ to 10.6 (9.63 h) for $\Delta_i = 1000$. 3) The depth of the upper layer in the frontal region is diminished (in order for w_e to become significant while Δ is still large). The minimum upper layer depth decreases from 0.08 (2.6 m) to 0.014 (0.46 m) for the DRM model and from 0.08 (2.6 m) to 0.03 (1 m) for the TLWE model. 4) The alongshore jet is augmented (Δ_x is bigger). For both models the magnitudes are approximately doubled; characteristic values for $\Delta_i = 180$ are 4 (12 cm/s) while for $\Delta_i = 1000$ they increase to about 10 (33 cm/s).

Figure 5

Temperature difference, Δ, lower layer potential vorticity, P, upper layer cross-shore and alongshore velocities, u_1 and v_1, and upper layer depth, h, obtained using the DRM model with $\Delta_i = 1000$ and $s = 0$. The times for the sequence shown are: 5a, 7.0 (6.42 h); 5b, 8.0 (7.33 h); 5c, 9.0 (8.25 h); 5d, 14.0 (12.83 h).

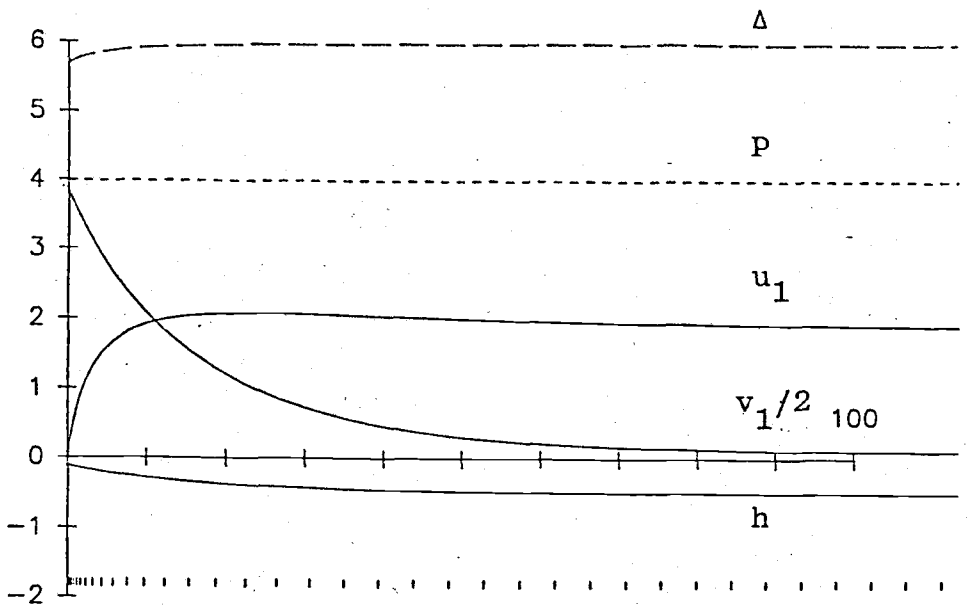

5a

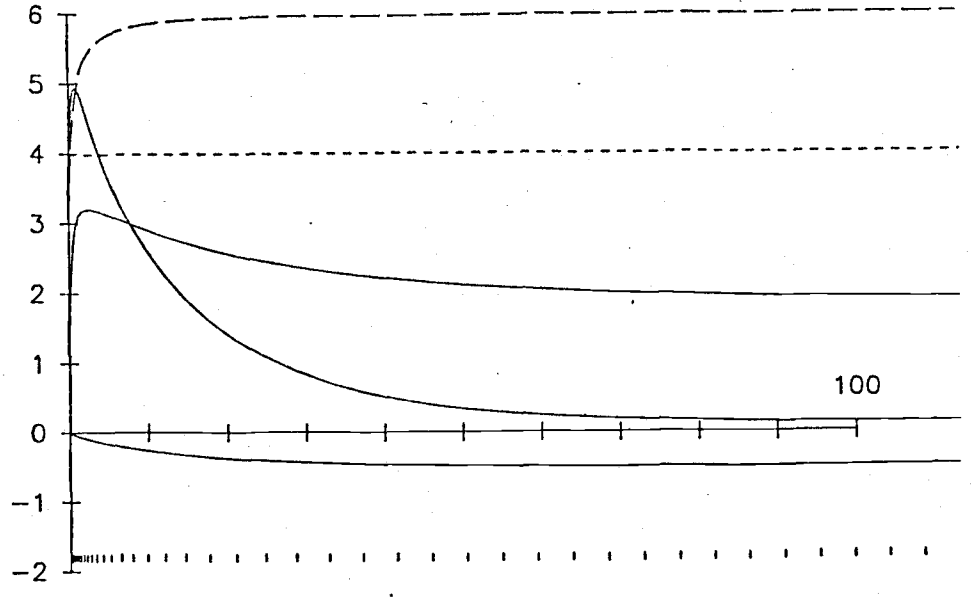

5b

Figure 5

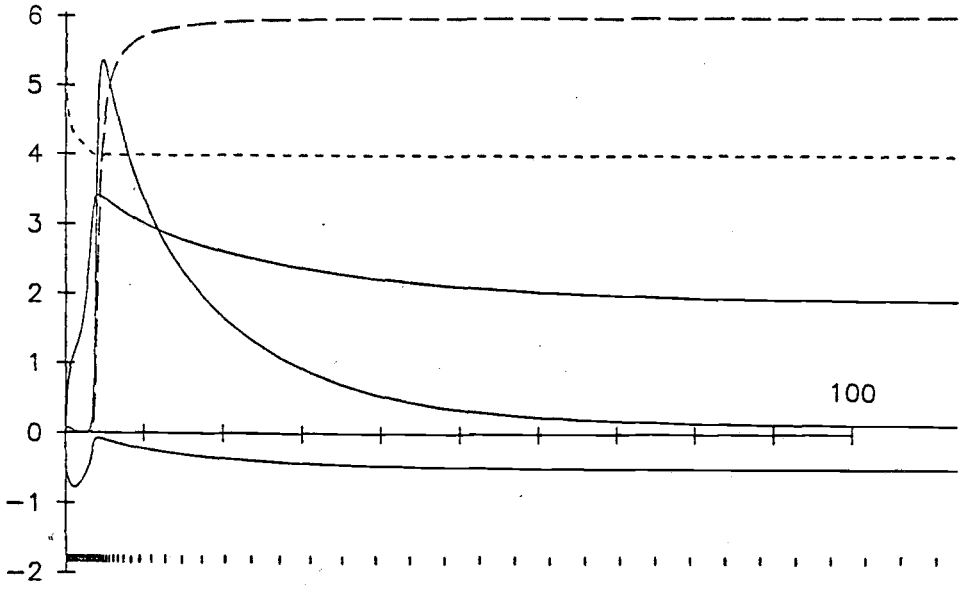

5c

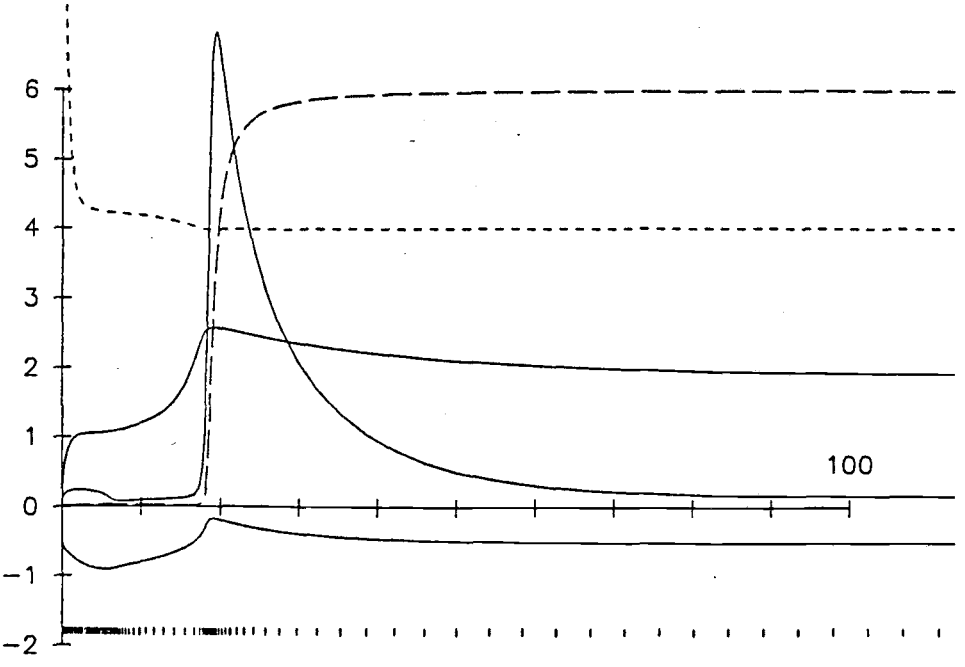

5d

Figure 5 (continued)

Figure 6

Temperature difference, Δ, interface elevation, η, entrainment velocity, w_e, and upper layer cross-shore and alongshore volume fluxes, U and V_1, obtained using the TLWE model with $\Delta_i = 1000$ and s = 0. The times for the sequence shown are: 6a, 7.0 (6.42 h); 6b, 11.0 (10.08 h); 6c, 12.0 (11.00 h); 6d, 14.0 (12.83 h).

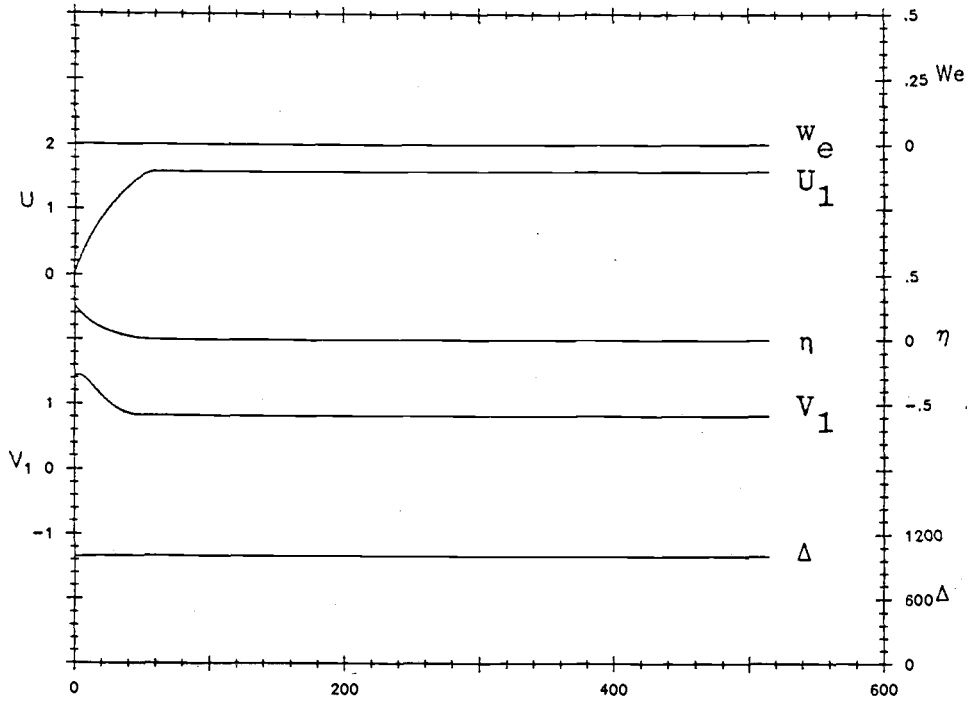

6a

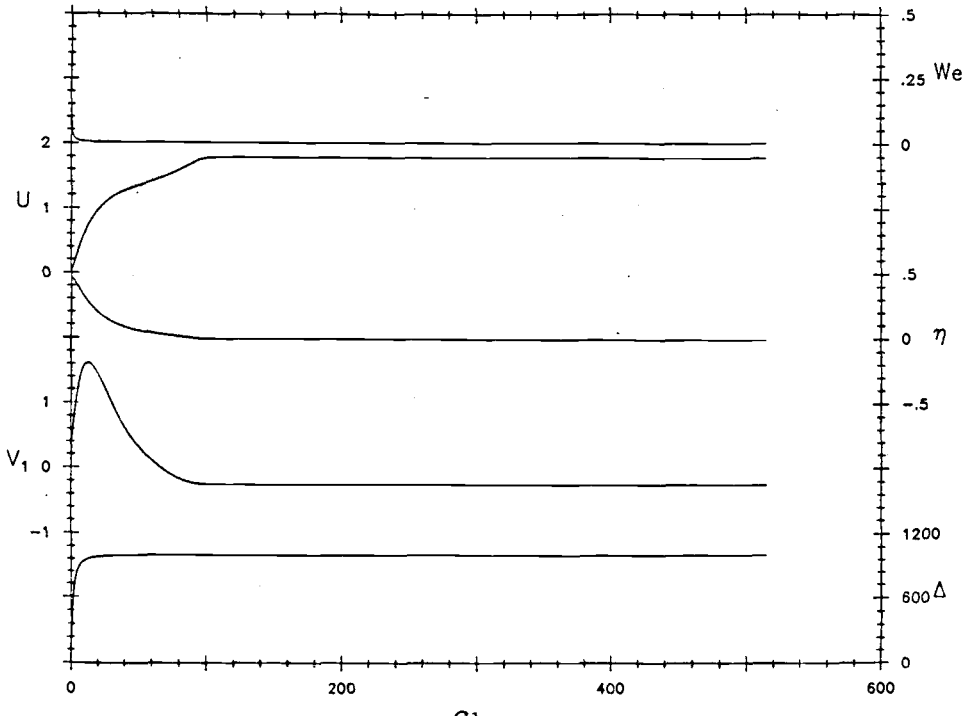

6b

Figure 6 (continued)

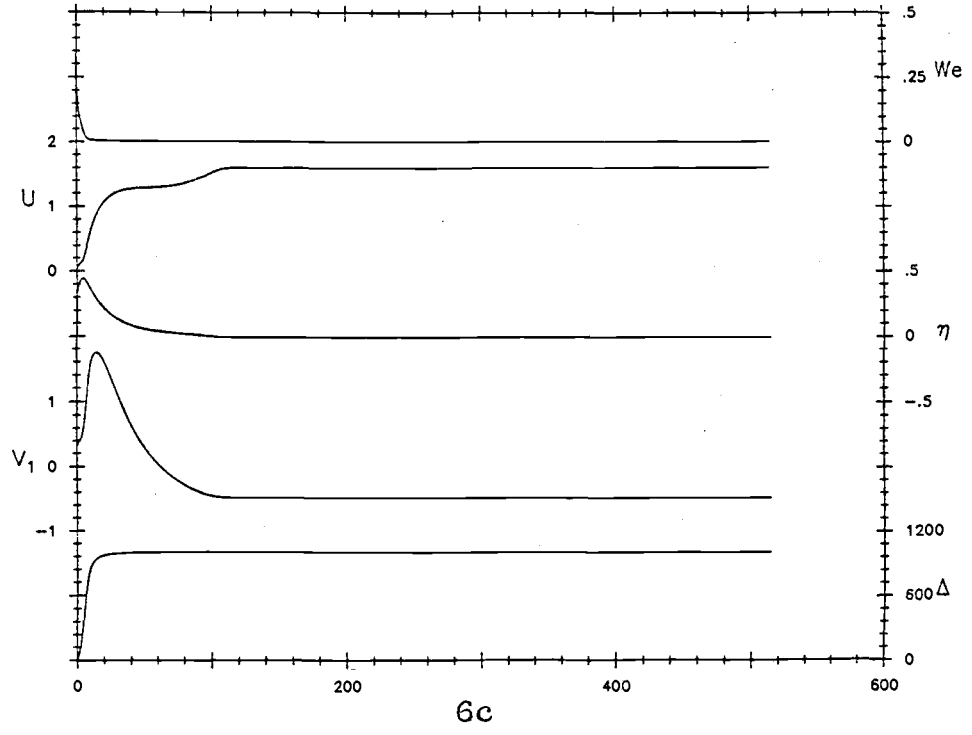

6c

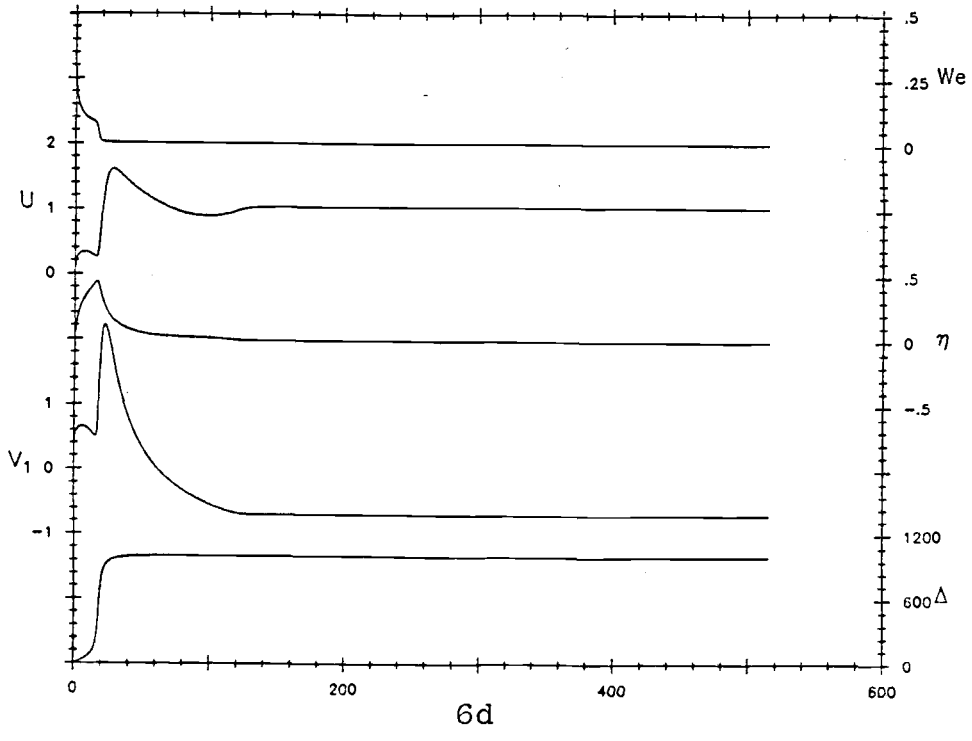

6d

Figure 6 (continued)

Figure 7

Temperature difference, Δ, interface elevation, η, entrainment velocity, w_e, and upper layer cross-shore and alongshore velocities, u_1 and v_1, for an expanded region near the coast, obtained using $\Delta_i = 1000$ and $s = 0$. The times for the sequence shown are: 7a, 7.0 (6.42 h); 7b, 11.0 (10.08 h); 7c, 12.0 (11.0 h); 7d, 14.0 (12.83 h).

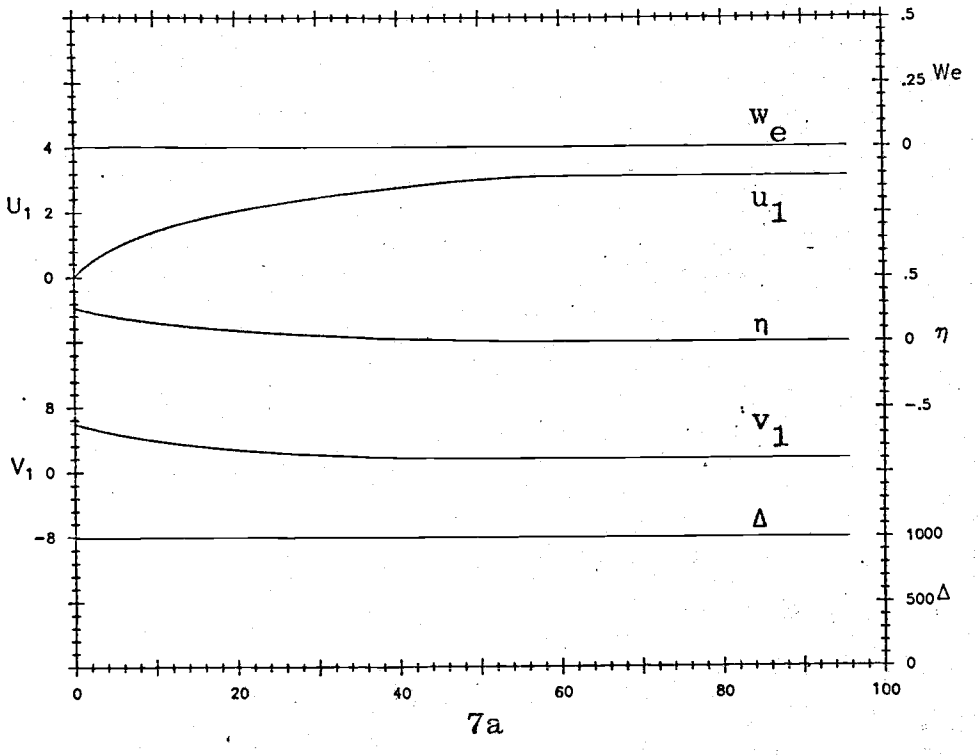

7a

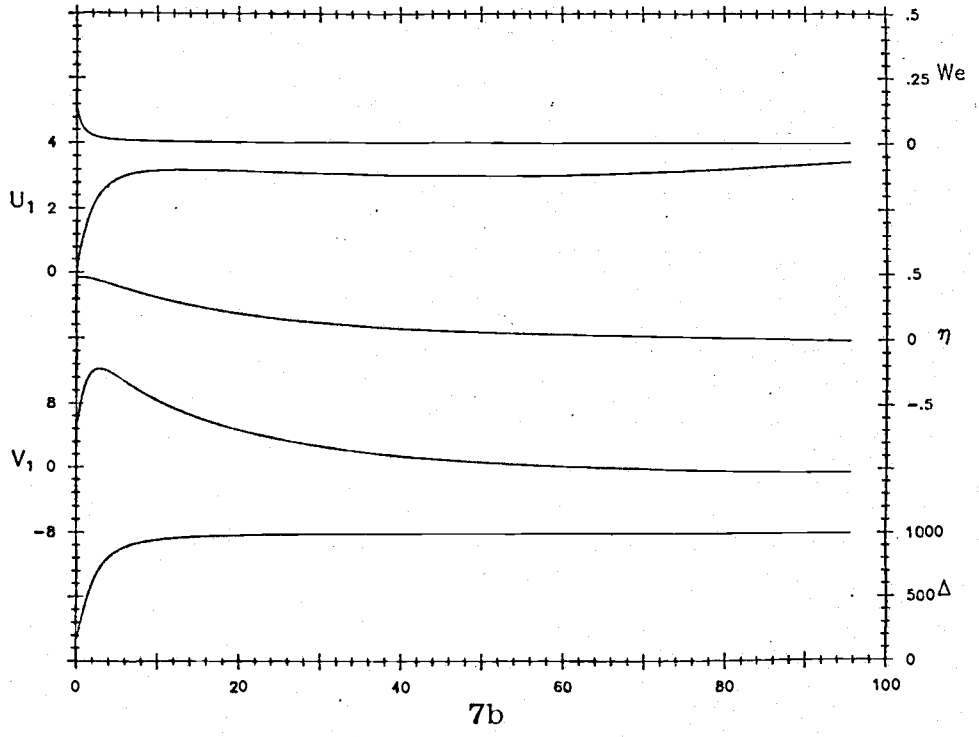

7b

Figure 7

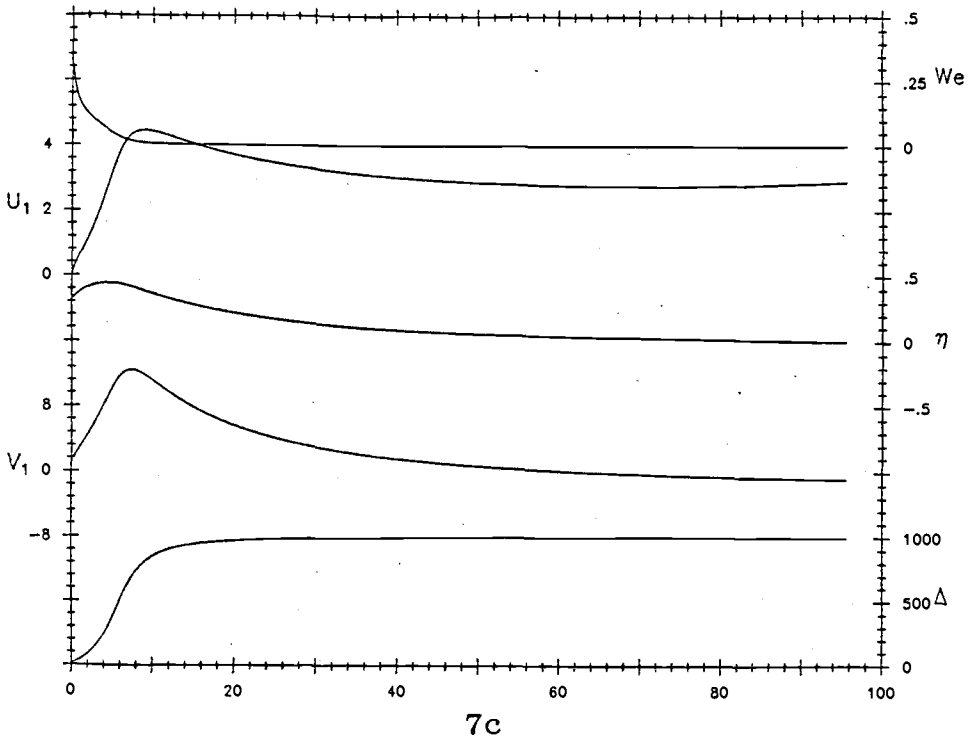

7c

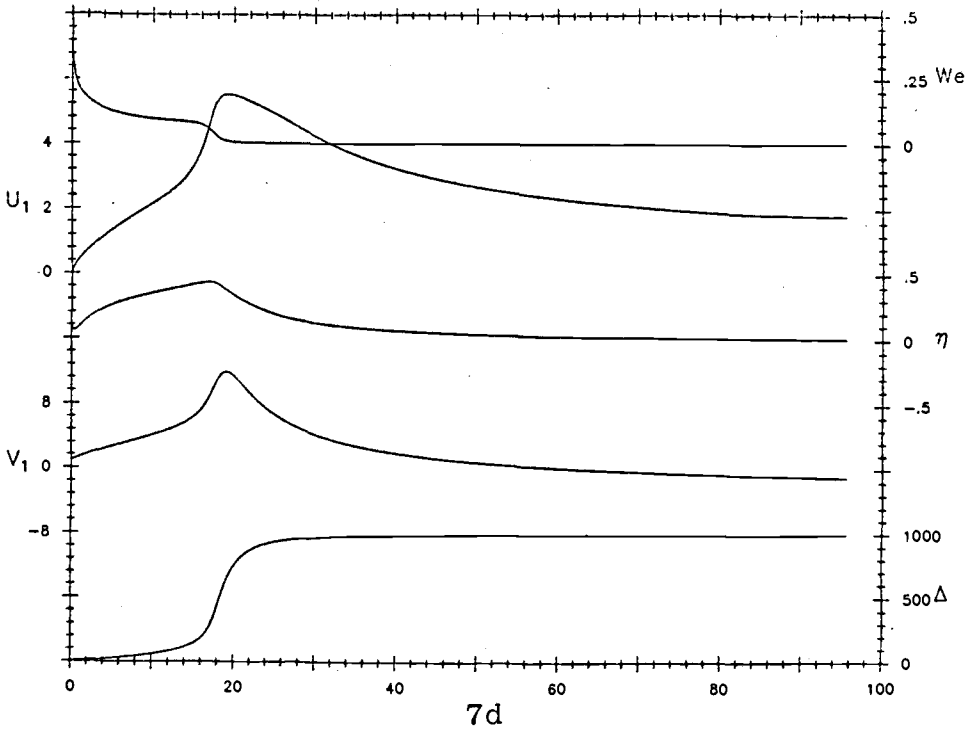

7d

Figure 7 (continued)

An interesting difference between the cases Δ_i = 180 (q = 2.5) and Δ_i = 1000 (q = 13.6) is the result of the inertial oscillations driving the horizontal flux divergence. For Δ_i = 180 the maximum offshore fluxes occur after $t_o = u_0 / \lambda_i$ while for Δ_i = 1000 they occur earlier. This causes that the delay in the upwelling time, due to the inertial oscillations, is much larger for the Δ_i = 180 case.

The results of the semigeostrophic model (DRM) with the shear enhanced entrainment formulation (s = 0.67), for Δ_i = 180, are shown in Figure 8. The importance of this mechanism can be observed by contrasting Figures 8 and 2. The main effect occurs at the frontal region where the alongshore jet resides (see, for example, Figures 2b and 8b, which correspond to the time 3.3 (3.03 h), when the thermocline surfaces). In this region w_e is enhanced by the shear mechanism which causes both Δ and v_1 to decrease, and the thermocline to upwell earlier.

The profiles for the TLWE model with s = 0.67 and Δ_i = 180, corresponding to the times 4.0 (3.67 h) and 5.0 (4.58 h), before and after the thermocline has surfaced, are shown in Figure 9. Shear due to the inertial oscillations enhances turbulence through the PRT mechanism causing significant entrainment velocities over the whole interior and frontal region (w_e is several times larger in the exterior region although it cannot be

Figure 8

Temperature difference, Δ, lower layer potential vorticity, P, upper layer cross-shore and alongshore velocities, u_1 and v_1, and upper layer depth, h, obtained using the DRM model with $\Delta_i = 180$ and s = 0.67. The times for the sequence shown are: 8a, 2.8 (2.57 h); 8b, 3.3 (3.03 h); 8c, 4.3 (3.94 h); 8d, 4.7 (4.31 h).

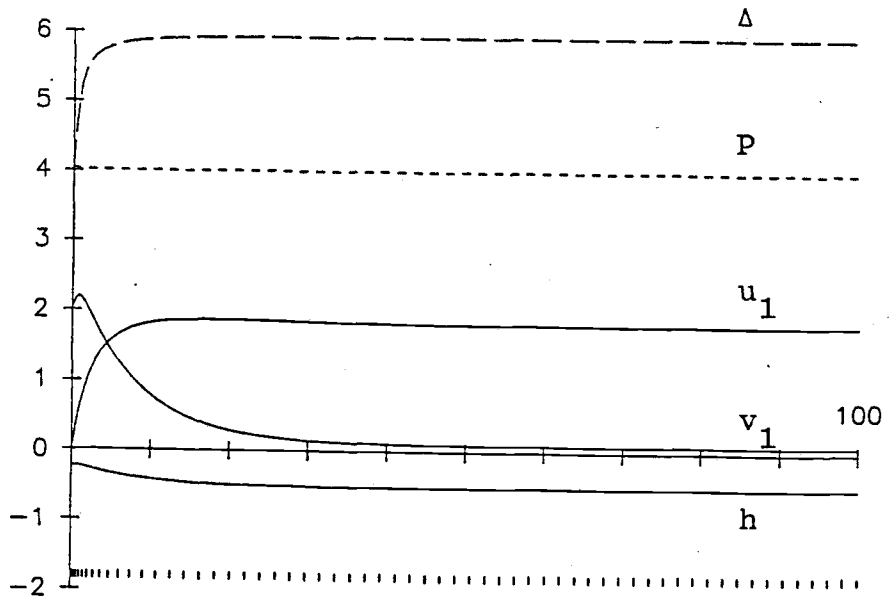

8a

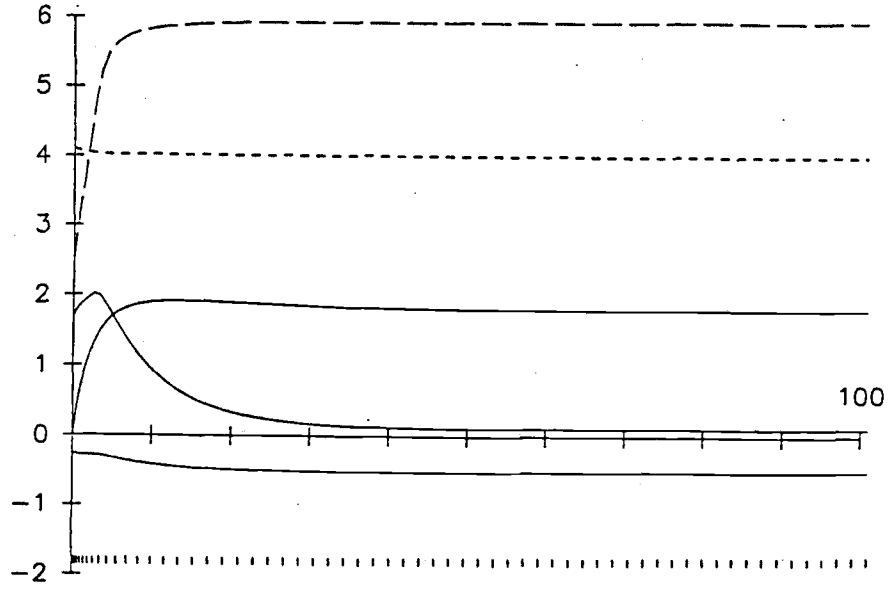

8b

Figure 8 (continued)

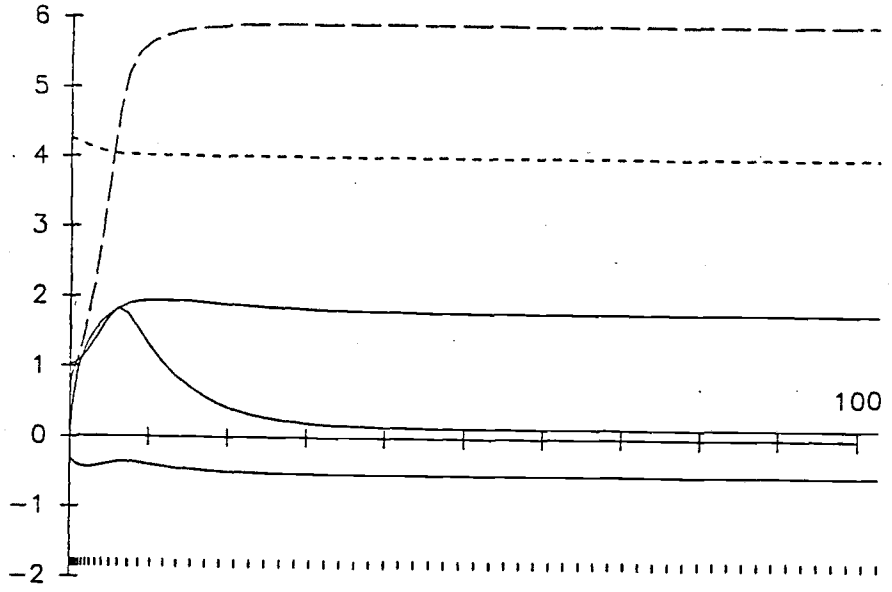

8c

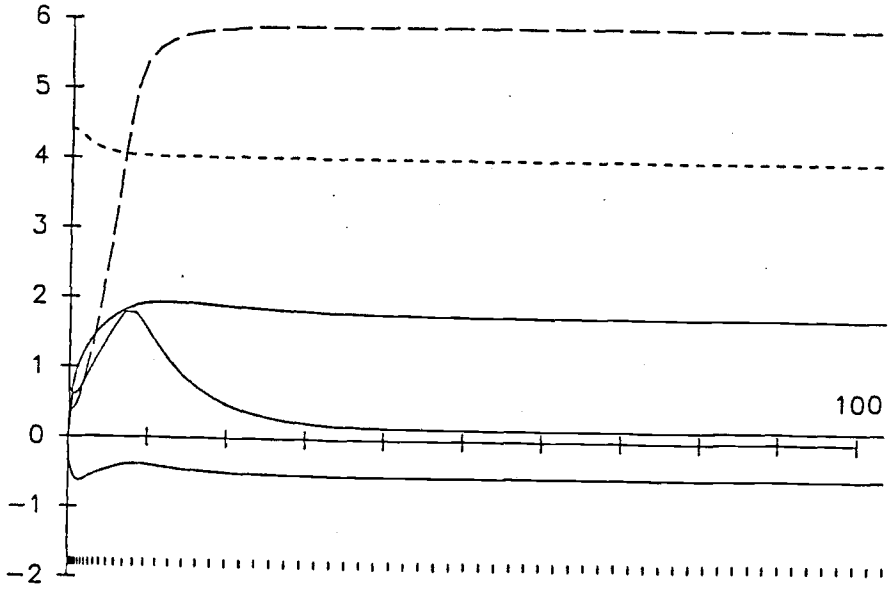

8d

Figure 8 (continued)

Figure 9

Temperature difference, Δ, interface elevation, η, entrainment velocity, w_e, and upper layer cross-shore and alongshore velocities, u_1 and v_1, for an expanded region near the coast, at times (9a) 4.0 (3.67 h) and (9b) 5.0 (4.53 h), obtained using the TLWE model with Δ_i = 180 and s = 0.67.

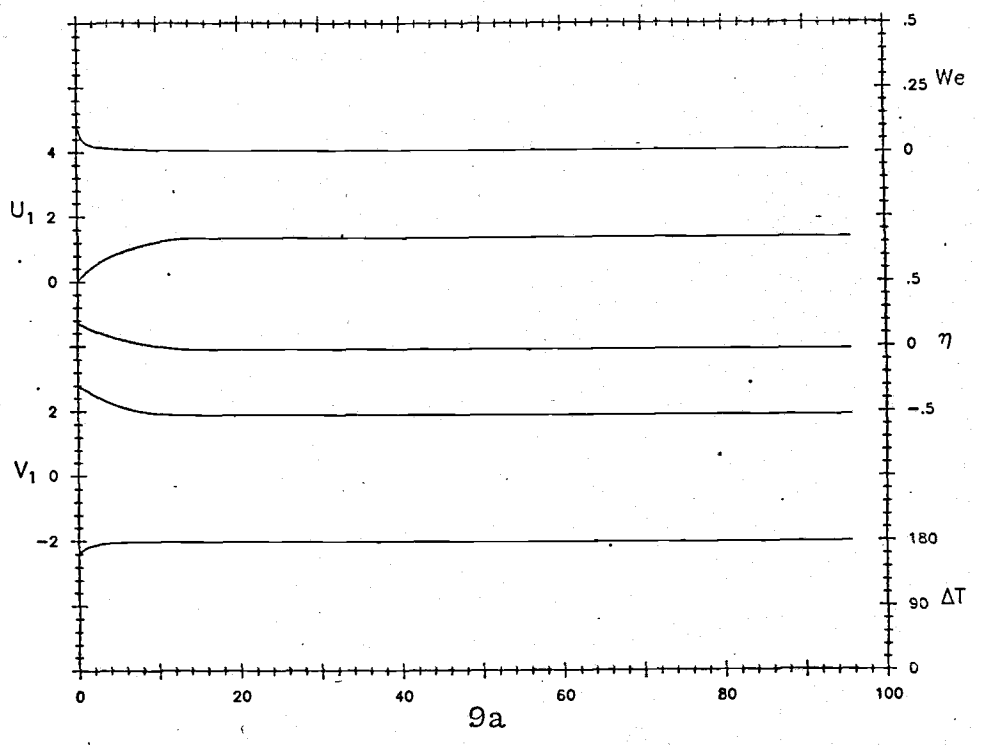

9a

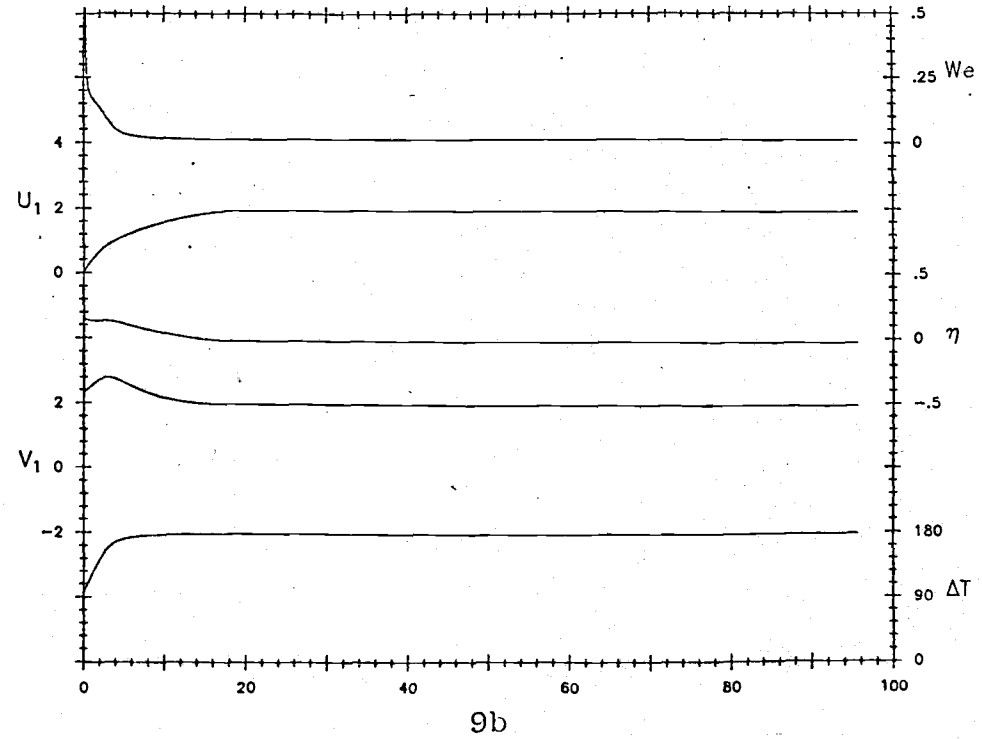

9b

Figure 9

distinguished from the plots). A clear manifestation of the importance of this mechanism comes from the minimum value taken by the upper layer depth. Without shear mixing the minimum upper layer depth is unaltered by the introduction of oscillations: 0.08 (2.6 m) for our computations with Δ_i = 180. When shear mixing is introduced (s = 0.67) the minimum upper layer depth increases to 0.23 (7.6 m) for the DRM model and to 0.30 (9.9 m) for the TLWE model.

The importance of the PRT mechanism could have been anticipated by looking at the values taken by the Richardson numbers at x = 1 (which is very close to the coast, ie. 100 For the case when s = 0 Ri very soon becomes supercritical, that is Ri_* becomes less than $0.67/ q^2$ = 6.03 (or equivalently, Ri goes under 0.67). Notice how also here the sharper character of the DRM front is manifested. In both models the minimum Ri occur just after the front upwells, and are due to the large shear associated with the alongshore jet over the frontal region. For the runs with s = 0.67 the Ri_* values become small less rapidly than before, and always remain subcritical, ie. above 0.67, showing the important role that shear-enhanced mixing plays in the system of equations (Figure 10).

The initial effect of the inertial oscillations on the divergence at the coast can be drawn from the simple

Figure 10

Richardson numbers as a function of time at x = 1.0 for four different cases: 1, DRM model with Δ_i = 180, s = 0.0; 2, TLWE model with Δ_i = 180, s = 0.0; 5, DRM model with Δ_i = 180 , s = 0.67; 6, TLWE model with Δ_i = 180, s = 0.67. Curve a corresponds to equation (56').

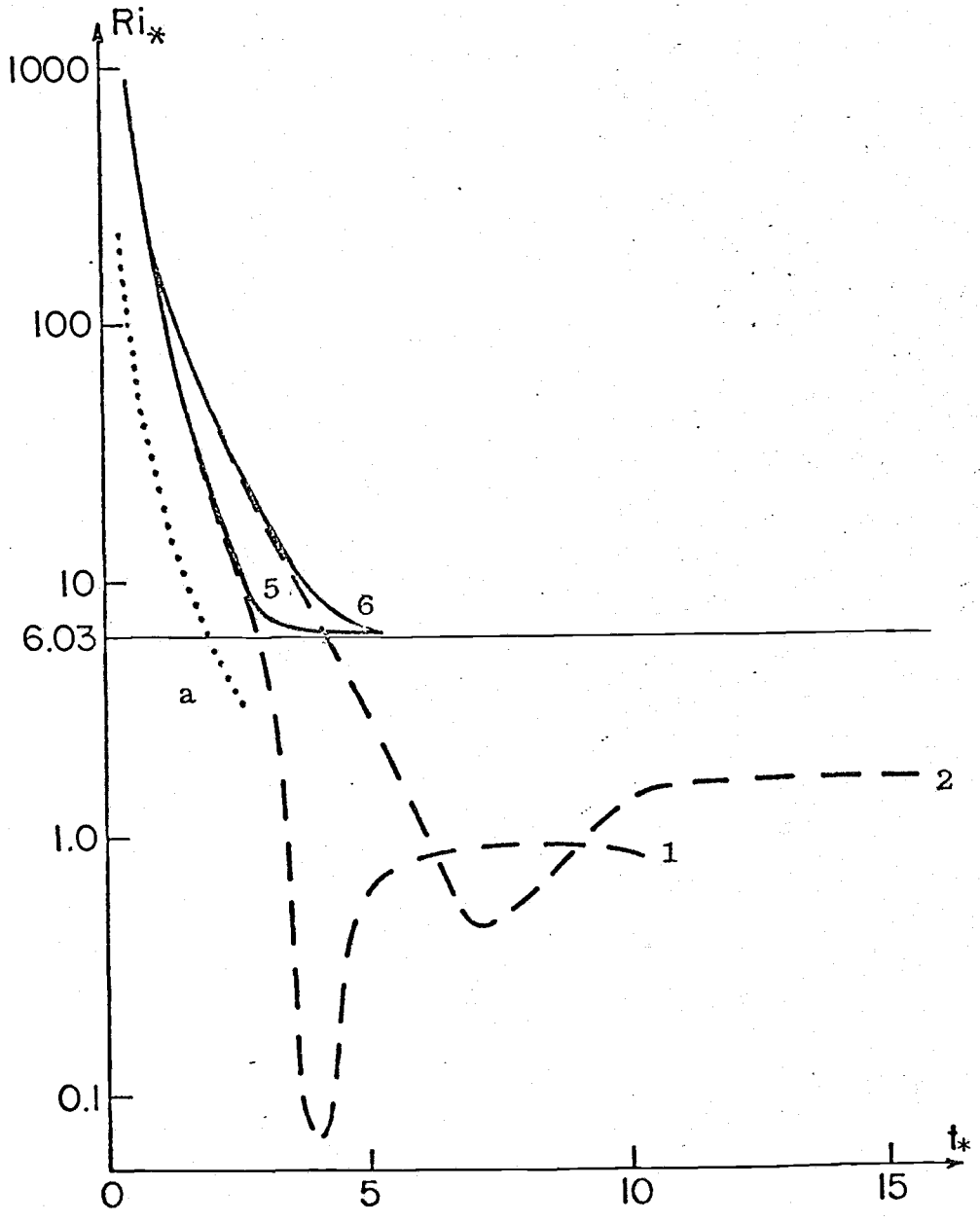

Figure 10

linear wind-driven inertial oscillation problem. In non-dimensional form it is

$$\frac{\partial U}{\partial t} - qV_1 = 0$$

$$\frac{\partial V_1}{\partial t} + qU = \tau \qquad (52)$$

whose solution far from the coast ($x >> \lambda_i = (\Delta_i h_i)^{\frac{1}{2}}$) is given by

$$U = \tau/q \quad (1 - \cos qt)$$

$$V_1 = \tau/q \quad \sin qt \qquad (53)$$

The condition of no normal flux at the coast requires the existence of an adjustment region. Following deSzoeke and Richman (1981) we can introduce it through the factor $(1 - e^{-x/\lambda i})$, which in non-dimensional form gives

$$U = \tau/q \ (1 - \cos qt) \ [1 - \exp(-x/(\Delta_i h_i)^{\frac{1}{2}})]$$

$$V_1 = \tau/q \ \sin qt \ [1 - \exp(-x/(\Delta_i h_i)^{\frac{1}{2}})] \qquad (54)$$

For this approximate solution the horizontal divergence of the cross-shelf volume flux is given by

$$U_x = \tau/q \ (1 - \cos qt) \ \exp[-x/(\Delta_i h_i)^{\frac{1}{2}}] \qquad (55)$$

This expression is approximately followed by our numerical solutions prior to the development of the front, as shown in the sequence of Figures 3b-3d. The effect of increasing Δ_i (i.e. to increase the length of adjustment) can be seen by comparison of these figures with Figure 6a. After the surfacing of the thermocline the interior quickly evolves towards a steady-state solution, ignorant of the evolution far offshore.

This same simple model could have anticipated the importance of the inertial oscillations in the shear mixing mechanism. Since the lower layer velocities are much smaller than the upper layer ones the shear across the interface can be approximated from (51) by $u_1^2+v_1^2$. Far offshore ($x >> \lambda_i$) this can be expressed as

$$(U/h)^2 + (V_1/h)^2 \approx \frac{2(1 - \cos qt)}{h_i^2} \qquad (56)$$

and its corresponding Ri_* is

$$Ri_* \geq \frac{\Delta_i h_i^3}{2(1 - \cos qt)} \qquad (57)$$

The minimum value for Ri_* occurs at $qt = \pi$, and is given by

$$\min \; Ri_* \approx \frac{\Delta_i h_i^3}{4} \tag{58}$$

For $h_i = 0.5$ and $\Delta_i = 180$ it gives a minimum Ri_* of 5.63 which is less than the critical Ri_* ($0.67/q^2 = 6.03$).

Close to the coast u_1 is small and the alongshore momentum balance can be approximated by

$$\frac{\partial V_1}{\partial \tau} \approx \tau \tag{59}$$

which for a constant wind stress gives

$$V_1 \approx \tau t \tag{60}$$

This shows that the alongshore jet approximately grows linearly in time as

$$v_1 \approx \tau t/h \tag{61}$$

For small times $h \approx h_i$ and the shear can be approximated by $(\tau t/h_i)^2$ which causes Ri_* to decrease very rapidly

$$Ri_* \approx \Delta_i h_i^3/(\tau t)^2 \tag{62}$$

This result has been plotted in Figure 10 (curve a). It suggests that the enhance mixing near the coast will be due predominantely to the alongshore jet. The quick decrease in the Ri_* for the DRM model is due to the immediate establishment of the offshore Ekman balance and fast development of the alongshore jet. Instead, the TLWE model shows larger Ri due to the longer time that it takes for the alongshore jet to develop.

The generation of internal waves (Poincare waves) at the coast has been discussed by Millot and Crepon (1981) and RA. RA have shown how the inertial motions are damped by these waves in several inertial periods. In the present work we have not considered them for two reasons. First, our numerical runs never lasted longer than one inertial period, t = 18.8 (17.23 h). Second, the small initial vertical stratification used results in a slow propagation of the Poincare waves, its maximum value being approximately given by

$$u_p = (\alpha g \Delta T_i h_1)^{\frac{1}{2}}$$

$$= q^2(\Delta_i h_i)^{\frac{1}{2}} v_* \qquad (63)$$

which for $\Delta_i = 180$ ($q = 0.33$, $h_i = 0.5$) results in $u_1 = 2.5v_*$. This value is usually smaller than the frontal velocity (which is equal to the cross-shore upper layer

velocity at the position of the front) as shown by Figures 2c-2d, 4c-4f. This indicates that for this case the damping of the inertial oscillations by the Poincare wave would be masked by the upwelled front. For $\Delta_i = 1000$ we get $u_1 = 13.6v_*$ while a characteristic value for the frontal speed is 10, which means that for this case the Poincare waves could be seen if the model ran for several inertial periods.

Figure 11 shows the position of the front as a function of time for both models, without the PRT mechanism. It can be observed that the velocity of propagation of the front for the TLWE model is more similar to that for the DRM model for the case with larger q_0. This goes in agreement with the behaviour indicated by RA , i.e. that the semigeostrophic (DRM) and inertial (TLWE) solutions become closer as q_0 increases.

Figure 11

Location in time of the front for four different cases: 1, DRM model with Δ_i = 180; 2, TLWE model with Δ_i = 180; 3, DRM model with Δ_i = 1000; 4, TLWE model with Δ_i = 1000 In all cases s = 0.0.

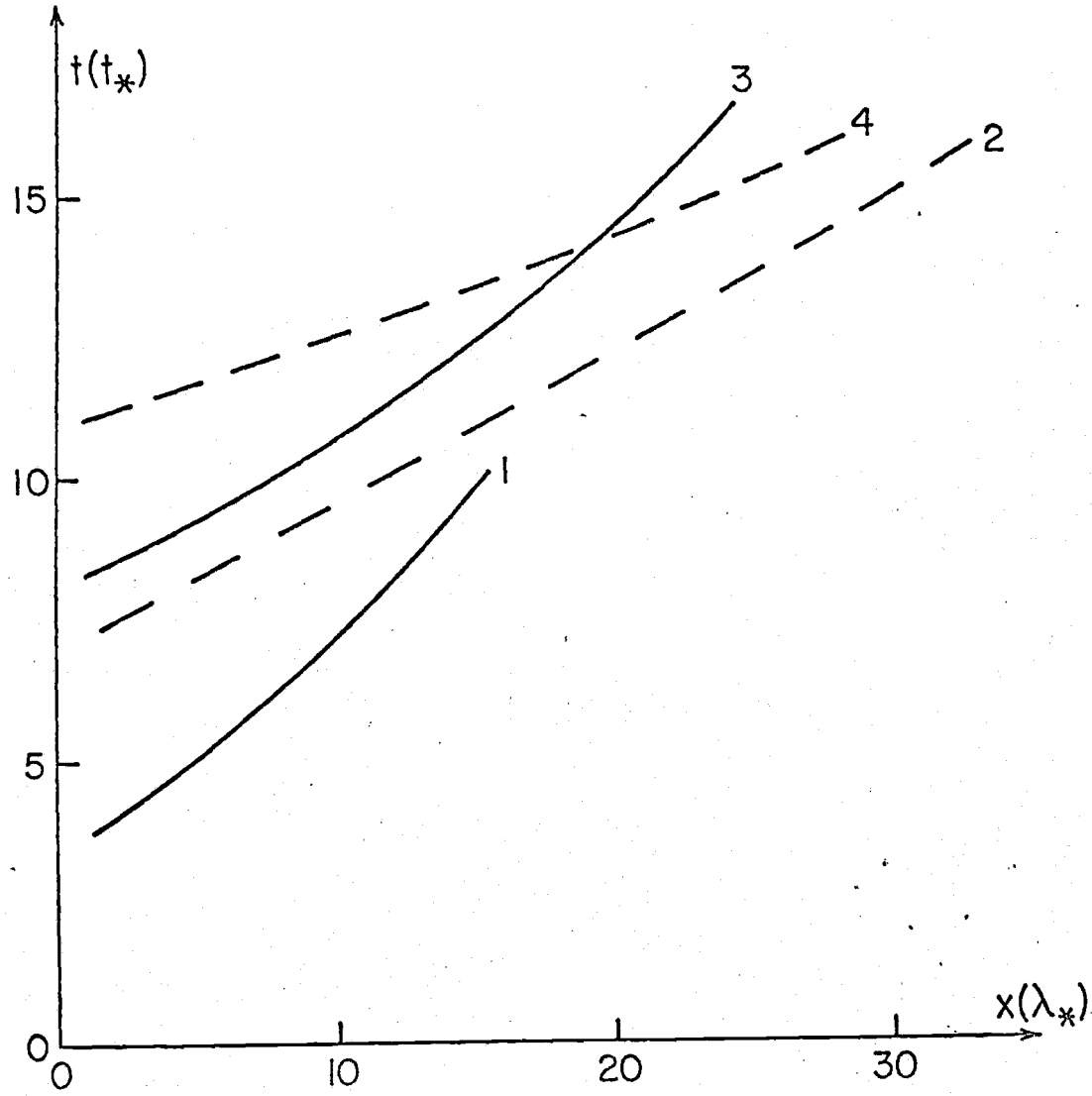

Figure 11

4. SUMMARY

A finite difference model has been succesfully employed to model coastal upwelling in the presence of inertial oscillations. By comparing the results from this model with those from the deSzoeke and Richman #(1984) model (modified to include shear enhanced mixing) the importance of the inertial oscillations during coastal upwelling has been analyzed. It has been determined that their effect is twofold: to modify the horizontal volume flux divergence at the coast and to enhance entrainment by shear-mixing.

It has been shown that the inertial oscillations change the divergence at the coast. One of the main effects is to increase the divergence over a larger area (the length of adjustment is increased); this causes the upper layer depth to decrease over this region, which enhances w_e, and ultimately acts to smooth the frontal characteristics. Another effect of the inertial oscillations comes from the variability that they have in the open ocean; this, together with the decoupling that exists within the upper layer at both sides of the front, causes the development of a shock-wave like phenomenon. This variability has other effects as to decrease the alongshore jet and to change the time at which the thermocline surfaces.

The enhancement of mixing by shear at the interface has been carefully studied and the role of inertial motions in this mechanism has been considered. In the absence of this mechanism the Richardson numbers, Ri, very soon become supercritical. The inclusion of this mechanism maintains Ri subcritical by increasing considerably the entrainment velocity. This causes upwelling to be substantially advanced and a further smoothing of the frontal features. The shear necessary for this mechanism is maximum over the frontal region where the alongshore jet occurs. However, inertial oscillations are responsible for the initial increase in the shear far away from the front. The enhancement of entrainment has a very important effect in the coastal dynamics; for example, it substantially decreases the alongshore jet.

From our results it can be concluded that both inertial oscillations and shear enhanced entrainment must be included in any realistic treatment of coastal upwelling.

BIBLIOGRAPHY

Allen, J. S., 1980: Models of wind-driven currents on the continental shelf. Annual Review of Fluid Mechanics, Vol. 12, Annual Reviews, Inc., 389-433.

Csanady, G. T., 1981: Circulation in the coastal ocean, Part 1. EOS Transactions, 62, 9-11.

Davis, R. E., R. deSzoeke and P. Niiler, 1981: Variability in the upper ocean during MILE. Part II: Modeling the mixed layer response. Deep Sea Res., 28 , 1453-1475.

DeSzoeke, R. A., 1980: On the effects of horizontal variability of wind stress on the dynamics of the ocean mixed layer. J. Phys. Oceanogr., 10, 1439-1454.

DeSzoeke, R. A., and J. G. Richman, 1981: The role of wind generated mixing in coastal upwelling. J. Phys. Oceanogr., 11, 1534-1547.

DeSzoeke, R. A., and J. G. Richman, 1984: On wind driven mixed layers with strong horizontal gradients - A theory with applications to coastal upwelling. J. Phys. Oceanogr., 14, 364-377.

Glimm, J., 1965: Solutions in the large for nonlinear hyperbolic systems of equations. Comm. Pure Appl. Math., 18, 197-715.

Kraus, E. B., and J. S. Turner, 1967: A one-dimensional model of the seasonal thermocline: II. The general theory and its consequences. Tellus, 19, 98-106.

Millot, C., and M. Crepon, 1981: Inertial oscillations on the continental shelf of the Gulf of Lions - Observations and Theory. J. Phys. Oceanogr., 11, 639-657.

Niiler, P. P., 1975: Deepening of the wind-mixed layer. J. Mar. Res., 33, 405-422.

Niiler, E. B., and E. B. Kraus, 1977: One-dimensional models of the upper ocean. In "Modelling and Prediction of the Upper Layers of the Ocean", E. B. Kraus, Ed., Pergamon Press, 143-172.

O'Brien, G. G., M. A. Hyman, and S. Kaplan, 1950: A study of the numerical solution of partial differential equations. J. Mathematics and Physics, 29, 223-251.

Pedlosky, J., 1979: "Geophysical Fluid Dynamics". Springer-Verlag, 624 pp.

Pollard, R. T., P. B. Rhines and R. O. R. Y. Thompson, 1973: The deepening of the wind-mixed layer. Geopphys. Fluid Dyn., 4, 381-404.

Price, J. F., C. N. K. Mooers and J. C. Van Leer, 1978: Observation and simulation of storm-induced mixed layer deepening. J. Phys. Oceanogr., 8, 582-599.

Richman, J. G., and J. S. Allen, 1984: Transient upwelling: a semigeostrophic adjustment problem. (submitted to J. Phys. Oceanogr.)

Thompson, J. D., 1978: Role of mixing in dynamics of upwelling systems. In "Upwelling Ecosystems", R. Boje and M. Tomczac, Eds., Springer-Verlag, 203-222.

APPENDICES

APPENDIX A. Finite Difference Scheme

The region of interest in the x-t space is covered by a rectangular grid with spacings Δx and Δt respectively. The value of any variable at a point ($x_m = m\Delta x$, $t_n = n\Delta t$) of the grid is denoted by

$$y(x_m, t_n) = y(m\Delta x, n\Delta t) \equiv y_m^n \qquad (A.1)$$

The time domain goes from t = 0 to a value large enough to show the main features of the evolving front. The space domain covers from the coast (x=0) to a distance far offshore where for all times considered the effects of the front are negligible (Figure A.1)

The values M, N such that $x_M = M\Delta x$ and $t_N = N\Delta t$ depend on the choices of Δx and Δt . The space intervals are given by

$$x_m = \begin{cases} 0.1\ \lambda_* , & 0<m<500 \\ 0.1\ (m-500)\ \lambda_* , & 500<m<550 \\ 5\ \lambda_* , & 520<m<620 \end{cases} \qquad (A.2)$$

This variation allows good resolution near the coast,

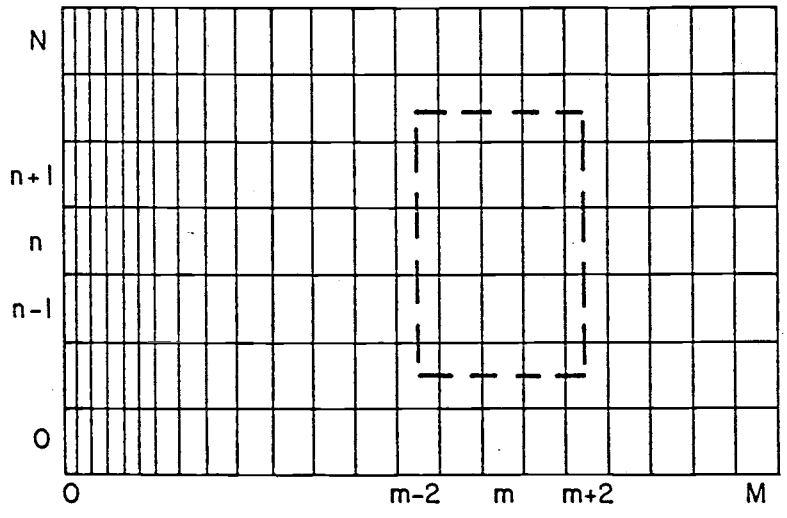

Figure A.1

Grid over the domain of interest (not to scale). The inner region is amplified in Figure A.2.

where the front evolves.

The time step Δ has to be small enough such that the numerical method is stable. For the near-linear problem it can be shown to depend on h_i , Δ_i , and q (see Appendix B).

Figure A.2 shows a small region of the grid with the cell structure employed for the variables appearing in equations (27)-(33). This particular structure is only one of the possible choices. It has been selected because it simplifies somewhat the finite difference representation of the equations. It also seems desirable to maintain U, V_1, V_2 together because of the similar character that they have in the momentum equations, and Δ , η , with w_e because of the interrelation shown in equation (33'). p_x has been more arbitrarily located with the volume transports.

The cell structure allows an easier use of a central difference approximation for for both the x and t derivatives. For example, equation (29) can be approximated by

$$\frac{U_{m+1}^{n+1} - U_m^{n+1}}{x_{m+1} - x_m} = \frac{\eta_m^{n+2} - \eta_m^n}{2\Delta t} + \frac{2}{\Delta_m^{n+1}} \left[\frac{\tau^{3/2}}{h_i - \eta_m^{n+1}} - Q\right] \qquad (A.3)$$

which after reordering becomes

$$\eta_m^{n+2} = \eta_m^n + \frac{2\Delta t(U_{m+1}^{n+1} - U_m^{n+1})}{x_{m+1} - x_m} - \frac{4\Delta t}{\Delta_m^{n+1}} \left[\frac{\tau^{3/2}}{(h_i - \eta_m^{n+1})} - Q\right] \qquad (A.4)$$

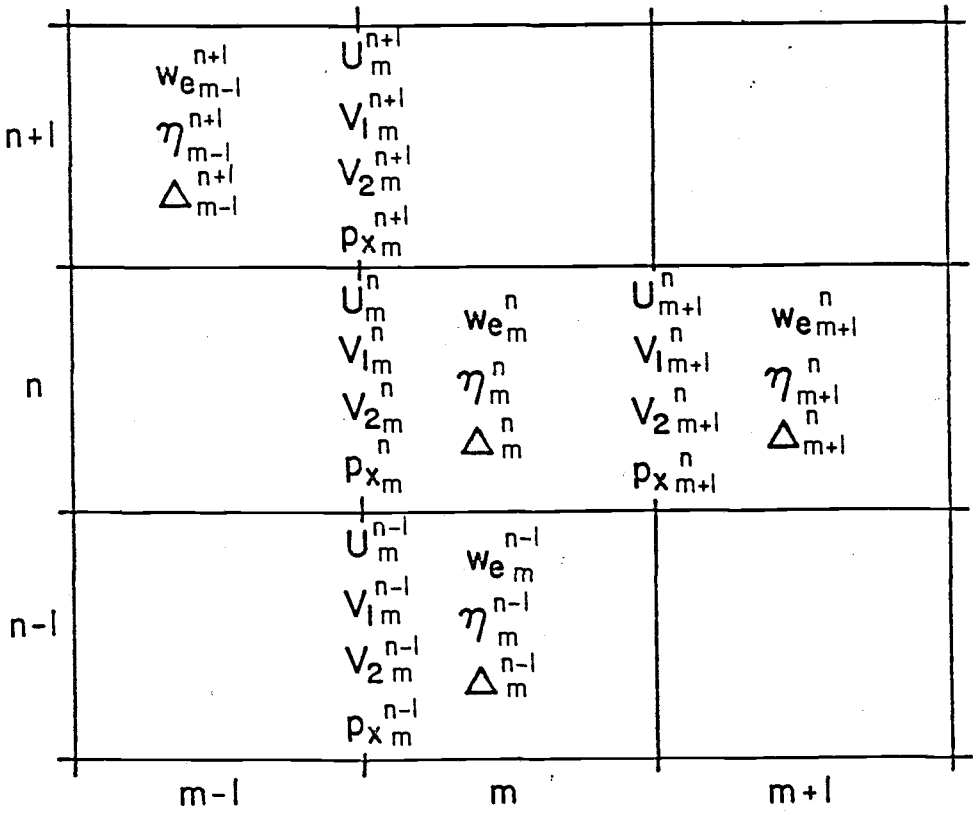

Figure A.2

Cell structure showing the positioning of the variables.

With a similar representation for all the equations and the knowledge of the initial and boundary conditions (see Section for 2.4) we can obtain an explicit solution for all variables, over the whole space domain, for successive time steps (in this treatment the coriolis terms in the momentum equations are treated implicitly).

APPENDIX B. Stability Analysis

The stability analysis for the system (27)-(33) has been done using the von Neumann method (O'Brien, Hyman and Kaplan, 1955). Since the applicability of this method is restricted to linear unforced systems the first step has been to linearize our system of equations. The linear system is

$$
\begin{aligned}
&V_{1_t} + qU = 0 \\
&U_t - qV_1 = -qh_i p_{o_x} \\
&\eta_t = U_x \qquad\qquad (B.1) \\
&V_{2_t} - qU = 0 \\
&p_{o_x} = \gamma(V_1+V_2) - q\Delta_i(1-\gamma h_i)\eta_x
\end{aligned}
$$

Notice that the equation for w_e is totally non-linear and for this reason does not exist in (B.1). Notice also that all forcing terms have been neglected, which reduces the heat equation to $\Delta = \Delta_i$.

In the von Neumann method all variables are written in terms of their Fourier series representation, eg.

$$U(m\Delta x,\ n\Delta t) \equiv U_m^n \equiv \sum_{k=1}^{K} U_k^m \exp(ik\pi m\Delta x/l) \qquad (B.2)$$

$$,\quad l = M\Delta x$$

and an amplification factor is introduced for the coefficients U_k^m

$$U_k^m = \xi U_k^{m-1} = \xi^m U_k^0 \qquad (B.3)$$

Since the finite difference equations are linear we need to study the stability for only one of the Fourier terms, say the first one (k=1). Hence, consider

$$U_m^n = U_1^0 \xi^n \exp(im\alpha) \quad , \qquad \alpha \equiv \pi\Delta x/l = \pi/M$$
$$= U_0 \xi^n \exp(im\ ) \quad , \qquad U_0 \equiv U_1^0 \qquad (B.4)$$

Similarly, let

$$V_{1_m}^n = V_{1_0} \xi^n \exp(im\alpha)$$
$$V_{2_m}^n = V_{2_0} \xi^n \exp(im\alpha)$$
$$\eta_m^n = \eta_0 \xi^n \exp(im\alpha) \qquad (B.4')$$
$$p_{x_m}^n = p_{x_0} \xi^n \exp(im\alpha)$$

The finite difference form of the system (B.1) is

$$
\begin{aligned}
U_m^{n+2} - q\Delta t V_{1_m}^{n+2} &= U_m^n + q\Delta t V_{1_m}^n - 2q\Delta t p_{x_m}^{n+1} \\
&= U_m^n + q\Delta t V_{1_m}^n - 2q\Delta t[\gamma(V_{1_m}^{n+1}+V_{2_m}^{n+1}) \\
&\qquad -(1-\gamma h_i)q\Delta_i\frac{(\eta_m^{n+1}-\eta_m^{n-1})}{\Delta x}] \\
V_{1_m}^{n+2} + q\Delta t U_m^{n+2} &= V_{1_m}^n - q\Delta t U_m^n \qquad \text{(B.5)} \\
\eta_m^{n+2} &= \eta_m^n + 2\Delta t/\Delta x \quad (U_{m+1}^{n+1} - U_m^{n+1}) \\
V_{2_m}^{n+2} - q\Delta t U_m^{n+2} &= V_{2_m}^n + q\Delta t U_m^n
\end{aligned}
$$

where the equation for p_x has been substituted into the U equation. Introducing (B.4) and (B.4') into (B.5) and dividing throughout by $\xi^n \exp(im\alpha)$ we get

$$
\begin{aligned}
U_0\xi^2 - q\Delta t V_{1_0}\xi &= U_0 + q\Delta t V_{1_0} - 2q\Delta t\gamma h_i\xi(V_{1_0}+V_{2_0}) \\
&\qquad + 2q^2(\Delta t/\Delta x)h_i(1-\gamma h_i)\Delta_i\xi\eta_0(1-e^{-i\alpha}) \\
V_{1_0}\xi^2 + q\Delta t U_0\xi^2 &= V_{1_0} - q\Delta t U_0 \qquad \text{(B.6)} \\
\eta_0\xi^2 &= \eta_0 + 2(\Delta t/\Delta x)U_0\xi(e^{i\alpha}-1) \\
V_{2_0}\xi^2 - q\Delta t U_0\xi^2 &= V_{2_0} + q\Delta t U_0
\end{aligned}
$$

which can be rewritten in matrix form as

$$A \begin{pmatrix} 0 \\ U_0 \\ V_{1_0} \\ V_{2_0} \end{pmatrix} = \begin{pmatrix} \xi^2-1 & -2(\Delta t/\Delta x)\gamma(e^{i\alpha}-1) & 0 & 0 \\ 0 & q\Delta t(\xi^2+1) & \xi^2-1 & 0 \\ -2q^2(\Delta t/\Delta x)h_i & \xi^2-1 & -q\Delta t(\xi^2+1-2\xi\gamma h_i) & 2q\Delta t\xi\gamma h_i \\ (1-\gamma h_i)\Delta_i\xi(1-e^{-i\alpha}) & & & \\ 0 & -\Delta tq(\xi^2+1) & 0 & \xi^2-1 \end{pmatrix} \begin{pmatrix} \eta_0 \\ U_0 \\ V_{1_0} \\ V_{2_0} \end{pmatrix}$$

$$= 0 \qquad \text{(B.7)}$$

(B.6) will have non-trivial solutions only if det A = 0. After some algebra we get

$$\det A = q^2\Delta t^2(\xi^4-1) + (\xi^2-1)^2 + 16q^2(\Delta t/\Delta x)\, h_i(1-\gamma h_i)\Delta_i\xi^2\sin^2\alpha/2 = 0 \qquad \text{(B.8)}$$

Let $|\zeta|=\xi^2$ to get an equation of the form

$$a\zeta^2 + b\zeta + c = 0 \qquad \text{(B.9)}$$

whose solution is

$$\zeta = \frac{-b \pm (b^2-4ac)^{\frac{1}{2}}}{2a} \qquad \text{(B.10)}$$

For stability we require that $|\zeta| < 1$, ie.

$$(2a + b)^2 > b^2 - 4ac$$
$$a + b > c \qquad \text{(B.11)}$$

For $\xi^2=+\zeta$ we get

$$a = q^2\Delta t^2 + 1$$
$$b = 16q^2(\Delta t/\Delta x)^2 h_i(1-\gamma h_i)\Delta_i \sin^2\alpha/2 = 2 \qquad \text{(B.12)}$$
$$c = 1 - q^2\Delta t^2$$

which leads to $\Delta t>0$. For $\xi^2=-\zeta$ we obtain

$$a = q^2\Delta t^2 + 1$$
$$b = 2 - 16q^2(\Delta t/\Delta x)^2 h_i(1-\gamma h_i)\Delta_i \sin^2\alpha/2 \qquad \text{(B.13)}$$
$$c = q^2\Delta t - 1$$

which gives $$t \leqslant \frac{\Delta x}{2q[h_i(1-\gamma h_i)\Delta_i]^{\frac{1}{2}}} \qquad \text{(B.14)}$$

The error introduced by the linearization is expected to be negligible as long as the non-linear terms are of the same order or smaller. In practice this appears to be true for most cases and the criterion given by equation (B.12) is satisfactory. However, there are two situations in which the above criterion fails. The first one corresponds to large times when an overtaking sharp front is formed (resembling a shock wave) and the non-linear terms become dominant. By decreasing the time step this difficulty is only delayed. This problem could probably be solved by employing a numerical scheme capable to deal with shock-wave type behaviour (see, for example, Glimm, 1965). The second situation arises for values of s (see Section 2.2) different of zero. In this case the system is unable to respond in a smooth and fast enough way to Richardson numbers approaching s, and quickly becomes unstable. A possible solution to this problem would be by reducing the time step when the difference (Ri - s) drops below some critical value. These limitations have not impeded us in studying some of the most interesting aspects of this problem and it has not seemed justified at this point to spend more effort on them.